Neural Networks 109 (2019) 113–136

Contents lists available at ScienceDirect

Neural Networks

journal homepage: www.elsevier.com/locate/neunet

# Roles for globus pallidus externa revealed in a computational model of action selection in the basal ganglia

Shreyas M. Suryanarayana [a], Jeanette Hellgren Kotaleski [a,b], Sten Grillner [a,*], Kevin N. Gurney [c]

[a] Department of Neuroscience, Karolinska Institutet, Stockholm, Sweden
[b] Science for Life Laboratory, School of Electrical Engineering and Computer Science, KTH Royal Institute of Technology, Stockholm, Sweden
[c] Department of Psychology, University of Sheffield, Sheffield, UK

ARTICLE INFO

*Article history:*
Received 27 June 2018
Received in revised form 28 August 2018
Accepted 9 October 2018
Available online 19 October 2018

*Keywords:*
Action selection
Network models
Globus pallidus externa
Arkypallidal GPe neurons
Prototypical GPe neurons

ABSTRACT

The basal ganglia are considered vital to action selection - a hypothesis supported by several biologically plausible computational models. Of the several subnuclei of the basal ganglia, the globus pallidus externa (GPe) has been thought of largely as a relay nucleus, and its intrinsic connectivity has not been incorporated in significant detail, in any model thus far. Here, we incorporate newly revealed subgroups of neurons within the GPe into an existing computational model of the basal ganglia, and investigate their role in action selection. Three main results ensued. First, using previously used metrics for selection, the new extended connectivity improved the action selection performance of the model. Second, low frequency theta oscillations were observed in the subpopulation of the GPe (the TA or 'arkypallidal' neurons) which project exclusively to the striatum. These oscillations were suppressed by increased dopamine activity — revealing a possible link with symptoms of Parkinson's disease. Third, a new phenomenon was observed in which the usual monotonic relationship between input to the basal ganglia and its output within an action 'channel' was, under some circumstances, reversed. Thus, at high levels of input, further increase of this input to the channel could cause an *increase* of the corresponding output rather than the more usually observed decrease. Moreover, this phenomenon was associated with the prevention of multiple channel selection, thereby assisting in optimal action selection. Examination of the mechanistic origin of our results showed the so-called 'prototypical' GPe neurons to be the principal subpopulation influencing action selection. They control the striatum via the arkypallidal neurons and are also able to regulate the output nuclei directly. Taken together, our results highlight the role of the GPe as a major control hub of the basal ganglia, and provide a mechanistic account for its control function.


## 1. Introduction

The basal ganglia are an evolutionarily conserved group of subcortical nuclei, which have long been implicated in action selection (Frank, 2005; Frank, Seeberger, & O'Reilly, 2004; Grillner & Robertson, 2016; Hikosaka, Takikawa, & Kawagoe, 2000; Lindahl, Kamali Sarvestani, Ekeberg, & Kotaleski, 2013; Redgrave, Prescott, & Gurney, 1999; Schroll, Vitay, & Hamker, 2012; Stephenson-Jones, Samuelsson, Ericsson, Robertson, & Grillner, 2011). Several computational models have been developed, examining their role in action selection (Berthet, Lindahl, Tully, Hellgren-Kotaleski, & Lansner, 2016; Frank et al., 2004; Gurney, Prescott, & Redgrave, 2001a, b; Hikosaka et al., 2000; Kamali Sarvestani, Lindahl, Hellgren Kotaleski, & Ekeberg, 2011; Mink, 1996; Schroll et al., 2012). They propose the basal ganglia as a 'selection machine' resolving conflicts between competing behaviours for common and restricted motor resources (Frank, 2005; Redgrave et al., 1999; Schroll & Hamker, 2013). This notion is backed by studies showing that the stimulation of the striatum, the main input nucleus, can either trigger actions or inhibit them (Freeze, Kravitz, Hammack, Berke, & Kreitzer, 2013; Kravitz et al., 2010). Furthermore, loss of dopamine neurons in the substancia nigra pars compacta (SNc), result in a reduced ability to select motor responses (Wylie et al., 2009) in pathological conditions like Parkinson's disease. In furtherance of the selection hypothesis, the basal ganglia are also implicated in learning of stimulus–response associations (Alexander, DeLong, & Strick, 1986) as well as in establishing stimulus–response–outcome associations (Redgrave & Gurney, 2006).

Existing models have dealt with a variety of aspects of basal ganglia function and anatomical context. Thus, many discuss the

* Corresponding author.
*E-mail addresses:* shreyas.suryanarayana@ki.se (S.M. Suryanarayana), jeanette@csc.kth.se (J. Hellgren Kotaleski), Sten.Grillner@ki.se (S. Grillner), k.gurney@sheffield.ac.uk (K.N. Gurney).

https://doi.org/10.1016/j.neunet.2018.10.003
0893-6080/

role of reinforcement learning (Brown, Bullock, & Grossberg, 2004; Frank, 2006; Gurney, Humphries, & Redgrave, 2015; Redgrave & Gurney, 2006; Schroll et al., 2012) and have also incorporated the thalamo-cortical loops (Beiser & Houk, 1998; Chersi, Mirolli, Pezzulo, & Baldassarre, 2013; Frank et al., 2004; Humphries & Gurney, 2002; van Albada & Robinson, 2009). These models also cover a range of levels of biological description — from abstract system-level to detailed multi-compartmental neuronal models, as well as simulations of ensembles of neurons. Addressing computations at the level of the subnuclei of the basal ganglia, there have been several models of the striatal microcircuitry (Damodaran, Cressman, Jedrzejewski-Szmek, & Blackwell, 2015; Humphries, Lepora, Wood, & Gurney, 2009; Humphries, Wood, & Gurney, 2009), the subthalamic nuclei (STN, Frank 2006), as well as examinations of the oscillations associated within the STN–GPe network (Blenkinsop, Anderson, & Gurney, 2017; Corbit et al., 2016).

Most models are based on the classical architecture of connectivity of the basal ganglia (Fig. 1(A)), focusing on the direct pathway – the striatal D1 projections to the output nuclei, globus pallidus interna and substantia nigra pars reticulata (GPi/SNr), and the indirect pathway – the striatal D2 projections to the GPe, and the GPe projections directly to GPi/SNr and the STN–GPe/GPi loop. The GPe has been considered as homologous in structure and function in most of these models. However, recent studies have revealed a new subpopulation of GPe neurons, the *arkypallidal* cells (Mallet et al., 2012) that are active in anti-phase to their more common counterparts, the *prototypical* GPe neurons (Mallet et al. 2012, see also Methods). These two classes are also referred to as the TA and TI neurons respectively (Mallet et al., 2012). The arkypallidal cells provide a major input to the striatum (Mallet et al., 2012).

We aimed to incorporate the arkypallidal neurons into a well-tested model architecture of the basal ganglia (Gurney et al., 2001a, b). The architecture has been validated at several levels of description: at the systems level using rate coded neural populations constrained by anatomical and physiological data (see Blenkinsop et al., 2017; Gurney, Humphries, Wood, J.Prescott, & P.Redgrave, 2004; Humphries & Gurney, 2002); spiking neuron models challenged with physiological data (Chersi et al., 2013; Humphries, Stewart, & Gurney, 2006; Stewart, Bekolay, & Eliasmith, 2012); and at the behavioural level in embodied (robotic) models (Prescott, Montes González, Gurney, Humphries, & Redgrave, 2006). Most recently, it has been used to link a raft of neurobehavioural phenomena to neuronal mechanisms observed *in vitro* (Gurney et al., 2015). Thus, this model architecture offers a strong platform to try to understand the role and function of arkypallidal neurons and their afferent and efferent pathways in action selection. Furthermore, we also included another scheme of organisation in the GPe in terms of neuronal subpopulations — the *outer* and *inner* GPe neurons (Sadek, Magill, & Bolam, 2007). We built on the original model and used the methodologies developed therein to assess them, on extended architectures of connectivity of the GPe. The arkypallidal neurons have been accommodated in a few computational models (Bahuguna, Tetzlaff, Kumar, Hellgren Kotaleski, & Morrison, 2017; Bogacz, Martin Moraud, Abdi, Magill, & Baufreton, 2016; Lindahl & Hellgren Kotaleski, 2016; Moolchand, Jones, & Frank, 2017) and their function in supporting optimal action selection (Bogacz et al., 2016) as well as in network dynamics underlying basal ganglia movement disorders have been investigated (Bahuguna et al., 2017; Lindahl & Hellgren Kotaleski, 2016). However, their role in action selection and their influence on other basal ganglia subnuclei, needs additional investigation. Further, the outer and inner neuron dichotomy has not been included in any model so far (to our knowledge), and their role in action selection remains unknown. Our work addresses these lacunas and reveals important functions for different neuronal subpopulations within the GPe, and unites these two prevalent schemes of organisation within the GPe (GPe TI/TA and GPe outer/inner, Mallet et al. 2012 and Sadek et al. 2007) and furthermore, places the GPe in perspective as an important control centre of the basal ganglia.

## 2. Materials and methods

### 2.1. Anatomy of the basal ganglia

The classical anatomy of the basal ganglia (Bolam, Hanley, Booth, & Bevan, 2000; Calabresi, Picconi, Tozzi, Ghiglieri, & Di Filippo, 2014; Redgrave et al., 1999) is shown in Fig. 1(A). It consists of the following principal nuclei: the striatum, the globus pallidus ((GPe) and internal (GPi) divisions in primates), the STN and the substantia nigra (SNr and SNc). The primary input nuclei are the striatum and the STN. The output nuclei are the GPi and the SNr. The input nuclei receive afferent signals from most of the cerebral cortex and the thalamus. The output nuclei project back to the thalamus, the superior colliculus and other mid-brain regions. The striatum projects to GPi/SNr as well as to the GPe. STN provides diffuse excitatory connections to the GPe and GPi/SNr. All other connections of the basal ganglia nuclei are inhibitory. The SNc provides dopaminergic input to the striatum, but is known to also project to other subnuclei of the basal ganglia (Bolam et al., 2000; Calabresi et al., 2014). There are two types of dopamine receptors associated with two subpopulations of the principal GABAergic projection neurons (>90%) in the striatum — the Striatal projection neurons (SPNs) or medium spiny neurons. One population, contains substance P and dynorphin, and preferentially expresses the D1-type of receptor, which facilitates cortico-striatal transmission. The other population contains enkephalin and preferentially expresses D2-type receptors, which attenuates cortico-striatal transmission (Akkal, Burbaud, Audin, & Bioulac, 1996; Harsing & Zigmond, 1997). The SPNs provide phasic inhibitory output through their efferents to the GPe and GPi/SNr.

#### 2.1.1. Anatomy of the GPe

Almost all of the GPe neurons are GABAergic except for a small subpopulation (∼5%) of cholinergic neurons which are sometimes regarded as an extension of basal forebrain cholinergic neurons (Abdi et al., 2015; Hernández et al., 2015; Mastro, Bouchard, Holt, & Gittis, 2014). The GABAergic GPe neurons were largely considered a homogeneous population until two schemes of population classifications emerged from the studies of Mallet et al. (2012) and Sadek et al. (2007). These two schemes form the basis for our modelling the GPe. New data from several studies have also subsequently contributed to the classification of GPe neuronal subtypes which we detail below.

*TI and TA neurons.* A hitherto unknown subpopulation of atypical GABAergic GPe neurons were first described by Mallet et al. (2012). The study dichotomises GPe neural population in Parkinsonian rats based on physiological behaviour. A major portion of GPe neurons (75%), discharge during the surface-negative component of cortical slow wave activity and are called GPe TI, Type I or 'prototypical' neurons. The other major portion (20%) of neurons, discharge during the surface-positive component of cortical slow wave activity, and are called GPe TA , Type A or 'arkypallidal' neurons. The GPe TI neurons give rise to projections which innervate the STN and GPi/SNr. Some of them also have modest projections to the striatum, which target the fast-spiking interneurons (FSNs, see also Glajch et al. 2016; Saunders, Huang, and Sabatini 2016). They also have extensive local axonal collaterals, targeting other TI neurons as well as GPe TA neurons. These neurons are parvalbumin positive and express the transcription factor Nkx2.1 (Abdi et al., 2015; Dodson et al., 2015). There is also a subset of these neurons which express Lhx6 (Abdi et al., 2015; Hegeman, Hong, Hernández, & Chan, 2016; Hernández et al., 2015). The firing pattern of the prototypical GPe cells is regular spiking (Abdi et al., 2015; Hernández et al., 2015). The GPe TA neurons on the other hand, are devoid of parvalbumin (Abdi et al., 2015; Hernández et al., 2015) and do not conform to this extrinsic axonal projection and do not

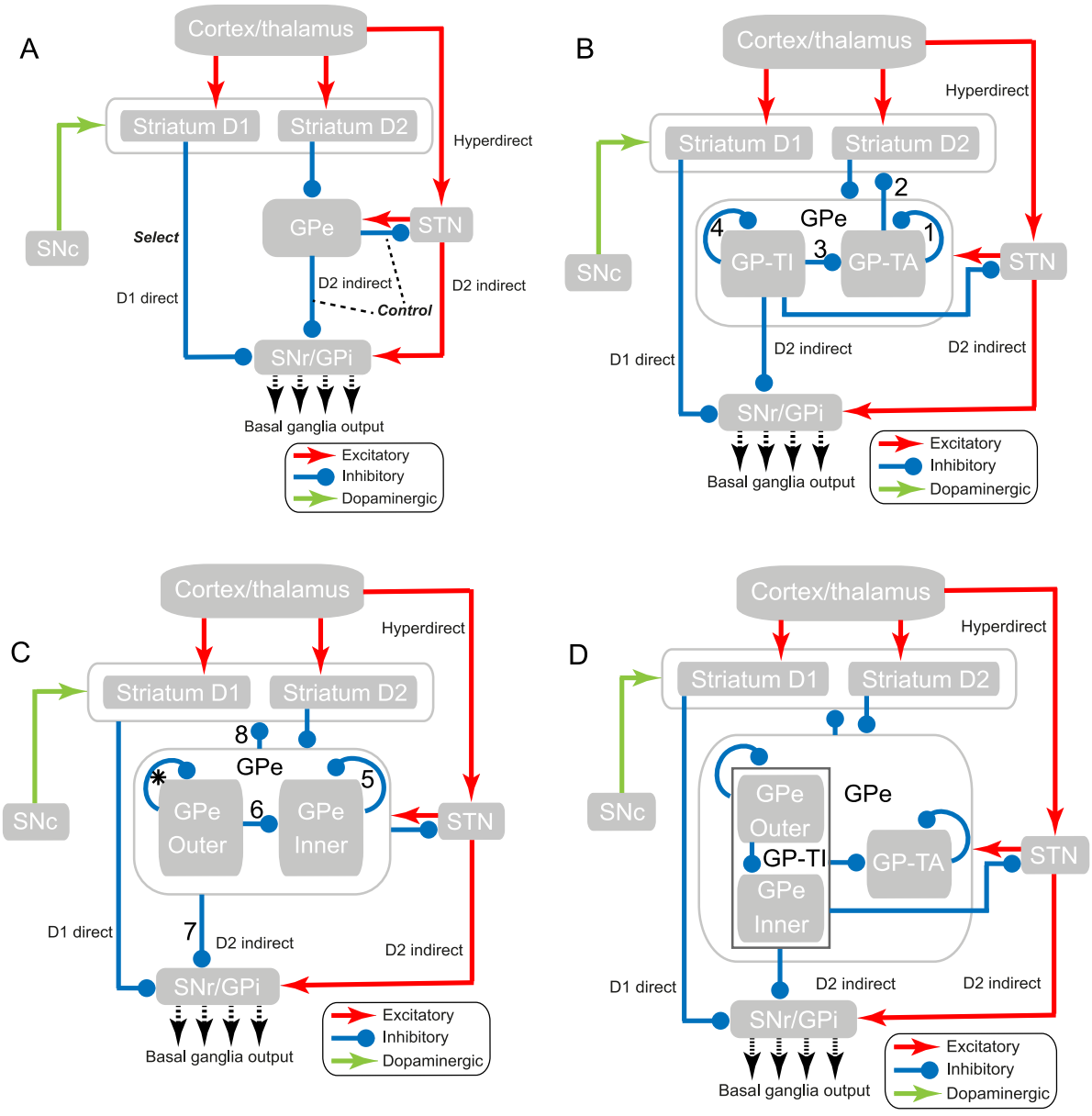


**Fig. 1.** *Basal ganglia connectivity.* (A) Functional architecture of the GPR model, showing the *selection* and *control* pathways. One component of the architecture — 'selection pathway' has its output as the GPi/SNr and the other component — 'control pathway' has its output as the GPe. (B) Architecture of connectivity within the basal ganglia, based on the intrinsic connectivity of the GPe, showing GPe TI and GPe TA neurons. The prototypical TI neurons project to the TA neurons and the GPi/SNr. They also project back to STN and have local collaterals amongst their own subpopulation. The TA neurons project exclusively to the striatum. The numbers (1–4) represent connections tested in step-wise models based on this scheme of connectivity. (C) Architecture of connectivity within the basal ganglia, based on the intrinsic connectivity of the GPe, showing outer and inner neurons. The outer neurons project to the inner neurons and both populations project to the STN and GPi/SNr. Both populations have projections to the striatum and finally, local collaterals amongst their own populations. The numbers (5–8) represent connections tested in step-wise models based on this scheme of connectivity. (D) The extended architecture of connectivity modelled in this study detailing the subpopulations within the GPe and unifying the GPe TA/TI and outer/inner schemes, is shown here. (For interpretation of the references to colour in this figure legend, the reader is referred to the web version of this article.)

have descending projections to either the STN or the GPi/SNr, but have long range axonal projections which provide a massive and dense innervation of the striatum (see also Glajch et al. 2016), along with local axonal collaterals. These cells express the transcription factors Npas1 and FoxP2 (Hegeman et al., 2016; Hernández et al., 2015; Mallet et al., 2012). The GPe TA neurons are thus described as a novel atypical neural population which do not conform to the premise that all GPe neurons invariably project back to the STN. The architecture incorporating the GPe TA/TI dichotomy is shown in Fig. 1(B).

*Outer and inner GPe neurons.* The other core aspect of our new modelling connectivity architecture is from the study of Sadek et al. (2007). Two neural subpopulations in the GPe have been described, based on their relative distance from the striato-pallidal border, and on the number of varicosities on their local axonal arborisations as the inner and outer neurons. The outer neurons are located closer to the striato-pallidal border ($<96\ \mu m$), and the inner neurons are located away from the striato-pallidal border ($\geq 96\ \mu m$). There is significant asymmetry in the connections of the two subpopulations. Inner neurons have more extensive local axonal collaterals, with neighbouring GPe neurons, and thus receive more input. The outer neurons substantially innervate the inner neurons, through axons traversing through the inner neuron regions on their way to the output nuclei. While a reverse *inner to outer* neuron connection exists, it is reportedly weak. Both the neural populations receive afferents from the striatum and STN

and have efferents back to the STN, as well as to the output nuclei GPi/SNr. This dichotomous clustering of the GPe outer and inner neurons, can be matched to the dual representation of the striatum in the GPe (Chang, Wilson, & Kitai, 1981). There is also mention of projections from both outer and inner neurons to the striatum. As a whole, about a third of the GPe neurons have projections to striatum. On cross-referencing with other studies, which reported projections of prototypical parvalbumin positive GPe neurons innervating the FSNs in the striatum (Bevan, Booth, Eaton, & Bolam, 1998; Glajch et al., 2016; Mastro et al., 2014; Saunders et al., 2016), we concluded that both the outer and inner neurons project to the striatal FSNs. The end effect of these projections being mediated via FSNs, would be reduction of FSN GABAergic inhibition of the SPNs (Szydlowski et al., 2013). The connectivity of the GPe with respect to other basal ganglia nuclei along with the dual representation of outer and inner neurons is shown in Fig. 1(C).

While the authors report that they have not correlated data across the two levels of organisation – the GPe prototypical, TI/arkypallidal, TA from (Mallet et al., 2012) and – the GPe outer/inner from (Sadek et al., 2007), following careful comparisons of the various studies described here, we concluded that the prototypical GPe TI neurons could be assumed to consist of both outer and inner GPe neurons. For instance, the axons of GPe TI neurons are quantitatively similar to the individual GPe neurons in dopamine-intact rats. Furthermore, the number of boutons on axonal projections in the striatum and STN of GPe TI neurons are well within the ranges of axonal boutons accounted for in single GPe prototypical neurons in dopamine-intact rats. The firing patterns of outer and inner neurons during cortical slow wave activity, which is said to be a highly regular single-spike pattern, matched with that of the GPe TI neurons. Striatal projections reported in the outer neurons (4 out of every 8 neurons), and in inner neurons (2 out of every 9 neurons), were also reported as modest striatal projections from GPe TI neurons. The GPe TA arkypallidal cells on the other hand, form a separate subpopulation.

Taking the anatomical considerations together, we propose the extended architecture shown in Fig. 1(D). We expand the connectivity of the GPe, by including the GPe TA neural subpopulation and its afferent and efferent connections, while the prototypical GPe TI neurons were accommodated in the modelling of outer and inner neurons.

### 2.2. Quantitative model development

#### 2.2.1. Existing model

We used the model by Gurney Prescott and Redgrave (Gurney et al., 2001a, 2001b) – henceforth referred to as the GPR model – as the basis for the extended architecture of connectivity modelled in this study. The architecture for the GPR model was based on the connectivity shown in Fig. 1(A). It included all the major pathways known at the time of its construction (for related review see Prescott, Gurney, and Redgrave 2002, see also Blenkinsop et al. 2017; Chersi et al. 2013; Gurney et al. 2004; Humphries and Gurney 2002; Humphries et al. 2006; Stewart et al. 2012) and provides a firm base for our model building. The assumption in the GPR model was that the brain processes a large number of sensory and cognitive streams or *channels* acting in parallel, each of them representing and requiring an action to be performed. To resolve the conflicts arising due to the processing in parallel of representations of different channels, it was proposed that the vertebrate brain has developed a 'central arbitrating mechanism' in which the 'urgency' or *salience* of the representations are supplied to a 'centralised arbitrator', which in turn selects the representation with the greatest salience, and to which motor (and possibly cognitive) resources are then allocated. The basal ganglia were hypothesised as this centralised arbitrator (Redgrave et al., 1999). A *functional architecture* with two components — 'selection pathway' and 'control pathway' (see Fig. 1(A)) was proposed, which demonstrated that the basal ganglia could perform action selection (Gurney et al., 2001a, 2001b). The role of the GPe in the GPR model was that of a 'regulator' of the selection pathway; the exact nature of the role was, however, not clear. By modelling the GPe, we have attempted to define that role more precisely, and tried to identify how various subpopulations within the GPe might contribute to that role.

The underlying assumption in the functional architecture was that an active representation of a putative action or *action request* (in cortex or subcortex) excites a population of neurons in striatum. This in turn, inhibits a corresponding population in GPi/SNr. This selective suppression of the tonic inhibitory control GPi/SNr normally exerts on its efferent targets, allows the action to be expressed. The combination of neural populations in various basal ganglia nuclei mediating an action request are said to comprise a processing *channel*. In addition, the STN also receives all action requests and supplies a diffuse excitation to GPi/SNr. In this way, striatum and STN comprise an off-centre, on-surround network that enables competitive processing between action channels. Each population in a channel, within a nucleus, was modelled by a single leaky integrator unit. Salience was represented as a scalar value at the input with one salience per channel. Selection in the model was defined with respect to a *selection threshold* in GPi/SNr such that, an output below this level was deemed to be associated with selection on the corresponding channel. In addition, a second, somewhat higher threshold — *distortion threshold*, allowed a subclassification of non-selected actions into those that are clearly playing no role in the current competition, and those which are just above the selection threshold, and which may *interfere* with selected actions, given small changes in salience. Further details are found in 'assessment and evaluation of selectivity' below. We now describe the model developed in this study.

### 2.3. Model formalisation

#### 2.3.1. Neuron model

All the models we describe make use of the leaky-integrator artificial neurons, which were used in the GPR model (Gurney et al., 2001b). We give a brief description of the same. The model will be made available on ModelDB. In each nucleus, the $i^{\text{th}}$ channel is represented by a single artificial neuron. The level of abstraction of the semilinear neuron means that it represents the population activity associated with the entire channel. If $u$ be the total afferent input to the artificial neuron, and if $k$ is a constant which determines the rate of activation decay, the total activation $\dot{a}$ of the leaky-integrator is given by:

$$\dot{a} = -k(a_i - u_i). \tag{1}$$

If $\tilde{a}$ is the activation at equilibrium, which is what we use in all our models, $\tilde{a} = u$. The output of the leaky-integrator denoted by $y$, is defined as a piecewise linear compression function, which ensures its value is bounded below by 0 and above by 1. The relation is given by:

$$y = m(a - \epsilon)H(a - \epsilon) \tag{2}$$

where $m$ is the slope of the output function, which is set to 1 in all our simulations.

$H(\,)$ is the Heaviside function, and $\epsilon$ is an activation threshold, below which, the output is zero.

#### 2.3.2. Synaptic weights

The synaptic weights associated with the different modelled pathways are listed in Table 1. The synaptic weight symbols have been named using a general mnemonic $W^{excitatory/inhibitory}_{source-destination}$.

**Table 1**
Synaptic weight symbols.

| Weight | Pathway |
|---|---|
| $w_i^{str}$ | Cortico-striatal weight for the $i^{th}$ channel |
| $w_{d2-ot}^-$ | Striatum D2 to GPe outer |
| $w_{d2-in}^-$ | Striatum D2 to GPe inner |
| $w_{d2-ta}^-$ | Striatum D2 to GPe TA |
| $w_{d1-snr}^-$ | Striatum D1 to GPi/SNr |
| $w_i^{stn}$ | Cortico-STN weight for the $i$th channel |
| $w_{stn-ot}^+$ | STN to GPe outer |
| $w_{stn-in}^+$ | STN to GPe inner |
| $w_{stn-ta}^+$ | STN to GPe TA |
| $w_{stn-snr}^+$ | STN to GPi/SNr |
| $w_{ot-d2}^-$ | GPe outer to striatum D2 |
| $w_{ot-d1}^-$ | GPe outer to striatum D1 |
| $w_{in-d2}^-$ | GPe inner to striatum D2 |
| $w_{in-d1}^-$ | GPe inner to striatum D1 |
| $w_{ot-stn}^-$ | GPe outer to STN |
| $w_{ot-snr}^-$ | GPe outer to GPi/SNr |
| $w_{in-stn}^-$ | GPe inner to STN |
| $w_{in-snr}^-$ | GPe inner to GPi/SNr |
| $w_{ta-d2}^-$ | GPe TA to striatum D2 |
| $w_{ta-d1}^-$ | GPe TA to striatum D1 |
| $w_{ta-ta}^-$ | GPe TA to GPe TA |
| $w_{ot-ot}^-$ | GPe outer to GPe outer |
| $w_{in-in}^-$ | GPe inner to GPe inner |
| $w_{ot-in}^-$ | GPe outer to GPe inner |
| $w_{ot-ta}^-$ | GPe outer to GPe TA |
| $w_{in-ta}^-$ | GPe inner to GPe TA |

Symbols used for synaptic weights of the different pathways modelled.

#### 2.3.3. Striatum

In the GPR model, the SPNs of the striatum have been modelled whereas the interneurons have been omitted. We limit to the modelling of SPNs here as well. The SPNs are divided into two populations, distinguished by the neurochemistry and response to dopamine which they receive from the SNc. This in turn divides the striatal model into two striatal sub-systems. The 'up/down' — state behaviour of SPNs, shifting between the more depolarised membrane potential – 'up' state, and the resting – 'down' state has been modelled by using a positive threshold in the output equation described in (2). Coming to the input to the striatum, we use a cortico-striatal weight $w_i^{str}$ for the $i^{th}$ channel. We now describe the dopamine input to striatum.

#### 2.3.4. Dopaminergic influence on selectivity

The role of dopamine in basal ganglia function was a pivotal aspect of this investigation. We have included dopaminergic influence through the innervations of the striatum by the SNc. While this influence is not modelled as a 'pathway' explicitly, we included dopamine influence with modulation of striatal weights. Dopaminergic influence has been reported in two instantiations, a short phasic burst (∼100 ms) and tonic activity (up to 8 Hz, Grace, Floresco, Goto, and Lodge 2007; Schultz 1998). We have modelled only the tonic level variations. We captured the difference in dopamine modulation on the D1 and D2 SPNs with dopaminergic transmission being facilitatory on D1 SPNs and cortico-striatal transmission being attenuated on D2 SPNs (Akkal et al., 1996; Harsing & Zigmond, 1997; Planert, Berger, & Silberberg, 2013). We replaced $w_i^{str}$ with $(1 \pm \lambda)w_i^{str}$, where $\lambda$ is the value of the tonic dopamine (see also Gurney, Prescott, and Redgrave 1998; Gurney et al. 2001b). To define the dopamine level, it was more instructive to consider a ratio of facilitation and attenuation — the *Dopamine ratio*, $R_w$ given by,

$$R_w = \frac{1+\lambda}{1-\lambda} \tag{3}$$

where, $0 \leq \lambda \leq 1$

#### 2.3.5. Modelled inputs

We summarise the modelled synaptic inputs for each subpopulation of neurons in various subnuclei of the basal ganglia. The activation function and the output relation as well as more details for each modelled subpopulation in all the nuclei can be found in the Appendix S1.

*Striatum D1.* The SPN D1 subpopulation in the striatum receives excitatory input from the cortex, diffuse inhibitory input from the GPe TA neurons, and the projections from the GPe outer and GPe inner neurons to striatum, as well as dopamine input from the SNc.

*Striatum D2.* The SPN D2 subpopulation in the striatum receives excitatory input from the cortex, diffuse inhibitory input from the GPe TA neurons, and the projections from the GPe outer and GPe inner neurons to striatum, as well as dopamine input from the SNc.

*STN.* The STN receives excitatory input from the cortex and inhibitory inputs from the GPe outer and GPe inner subpopulations.

*GPe outer (part of GPe TI).* GPe outer neurons receive diffuse excitatory input from the STN, inhibitory input from the striatum SPN D2 and inhibitory local collaterals from other GPe outer neurons.

*GPe inner (part of GPe TI).* GPe inner neurons receive diffuse excitatory input from the STN, input from the striatum SPN D2 and local inhibitory collaterals from other GPe inner neurons. Additionally, they also receive processed input from the GPe outer neurons.

*GPe TA.* GPe TA neurons receive diffuse excitatory input from the STN, input from striatum SPN D2 neurons, local inhibitory collaterals from GPe outer and GPe inner neurons along with local inhibitory collaterals from other GPe TA neurons.

*GPi/SNr.* The output nuclei receive inhibitory input from the striatum SPN D1 neurons, diffuse excitatory input from the STN along with inhibitory inputs from the GPe outer and GPe inner neuron subpopulations.

### 2.4. Parameter values

The fixed parameter values included the thresholds for different neuronal subpopulations and some synaptic weights. They were chosen based on the criteria set out in the GPR model (Gurney et al., 2004, 2001b). Most of the synaptic weights and thresholds associated with the GPR model nuclei were simply extended to new neural populations. The rate constant $k$ in Eq. (1) was set at 25 (equivalent to a neural membrane time constant of 50 ms), and the slope for each nuclei $m$, was set to 1 (see Gurney et al. 2001b). The thresholds associated with different subnuclei are given in Table 2. All the synaptic weights which were fixed, are shown in Table 3. The simulations also required varying a number of synaptic weights and combinations of synaptic weights from different pathways for trying to understand functions of different pathways. The weights were varied in steps of 0.25, between 0 and 1, except for the GPe pathway weights to the GPi/SNr, which were varied in steps of 0.2.

### 2.5. Simulations — guiding principles

The original GPR model had shown that the basic basal ganglia connectivity architecture when investigated from a systems-level, can behave like an effective selection mechanism. We incorporate more biological detail into the model, and are guided by the following principles while simulating and evaluating the model.

**Table 2**
Thresholds.

| | | | |
|---|---|---|---|
| $\epsilon_{str}$ | 0.2 | $\epsilon_{in}$ | −0.2 |
| $\epsilon_{stn}$ | −0.25 | $\epsilon_{ta}$ | −0.2 |
| $\epsilon_{ot}$ | −0.2 | $\epsilon_{snr}$ | −0.2 |

Threshold values of the various nuclei and neural subpopulations used in the model.

**Table 3**
Fixed synaptic weights.

| | | | |
|---|---|---|---|
| $w_i^{str}$ | −1 | $w_i^{stn}$ | 1 |
| $w^-_{d2-ot}$ | −1 | $w^+_{stn-ot}$ | 0.8 |
| $w^-_{d2-in}$ | −1 | $w^+_{stn-in}$ | 0.8 |
| $w^-_{d2-ta}$ | −1 | $w^+_{stn-ta}$ | 0.8 |
| $w^-_{d1-snr}$ | −1 | $w^+_{stn-snr}$ | 0.9 |

Synaptic weights of the pathways used in the model, which were fixed.

#### 2.5.1. Enhancement of selectivity

The model is driven by the hypothesis that action selection is a primary function of the basal ganglia connectivity architecture, and with more biological detail we incorporate, there must be an enhancement of the ability of the model to select. Selectivity is essentially the ability of the model to 'choose' an action representation with the highest salience in a competition between different action representations. We define a metric to quantify selection and evaluate it, which is detailed in subsequent sections.

#### 2.5.2. Mechanisms underlying selectivity

Incorporation of significant biological detail also required us to investigate whether new mechanisms of enforcing selectivity were generated. We observed for instance, in some models with the extended connectivity, there was a decrease in the channel output with increasing salience, which could prevent the selection of that channel. 'Reversal', as we called this mechanism — was a new way through which the system could enforce selections in specific cases of conflict. Reversal was able to resolve a conflict between two representations with high salience (see also Section 2.7.6).

#### 2.5.3. Roles of pathways

The extended connectivity resulted in addition of a large number of biologically grounded pathways. A primary question we addressed here, was to look into how these individual pathways contributed to action selection. This was extended subsequently to neural populations and then to the entire subnucleus (GPe).

#### 2.5.4. Role of dopamine

Dopamine plays a crucial modulatory role in the basal ganglia, and to investigate its influence on selection was another major goal of the simulations. We investigated the consequences of different degrees of dopaminergic modulation in the striatum for each new pathway modelled. This was pertinent, since dopamine loss and resultant oscillatory activity in the basal ganglia underlies several pathological conditions like Parkinson's. The aim was to investigate dependency of selection on dopamine, but also to try to dissect out circuits which caused oscillatory activity during lack of dopamine modulation.

### 2.6. Experimental strategy

The lack of decisive empirical evidence on the connectivity of the newly discovered GPe sub-populations means that there is a proliferation of possible pathways, consistent with the data. We therefore sought to investigate, as far as possible, the role of individual pathways before bringing them together into a more realistic, but complex, configuration. We achieved this by running a series of *Step-wise models* which simulated individual connections/pathways added to the GPR model. The Step-wise models allowed us to tease out the contribution of every new pathway we simulated, in action selection, from the new connectivity scheme we added on in the GPe (See Fig. 1(D)). This resulted in a Step-wise model for each new pathway modelled (and named based on the pathway modelled) and whose performance was evaluated and compared with the original GPR model (See Figs. S1 & S2). Thus, for each subpopulation of GPe, there are projections to other basal ganglia nuclei, projections to other GPe subpopulations, and projections within the same population. Then, in a series of *Combined models*, we combined connections in stages to simulate first, the entire projective connectivity of each subpopulation, before repeating this with multiple subpopulations together. This enabled us to determine the functions for the various pathways and subpopulations of the GPe, as well as draw conclusions on the function of the GPe as a whole. Consequently, we present the simulation results broadly in three phases. In the first phase, we show step-wise models for the GPe TA subpopulation. In the second phase, we show a similar set of simulations of the GPe TI subpopulation. In the final phase, we draw these two subpopulations together in different ways into the extended architecture of GPe connectivity shown in Fig. 1(D).

### 2.7. Assessment and evaluation of selectivity

In order to assess the capabilities of each model variation, we established several metrics that described 'selectivity'. Their definition builds on a simple pairwise competition protocol, the notions of 'hard' and 'soft' selection, and how these modes of selection vary with dopamine. We now describe the metrics and their construction in detail.

#### 2.7.1. Basic selection procedure

In our simulations, we have actively driven two channels in a six channel model to replicate the stimulus protocols used in characterising the original GPR model (Gurney et al., 2004, 2001a). Selection was explored using a fixed protocol of salience variation of the two active channels (Fig. 2). The selection threshold ($\theta_s$) was set to 0 and the distortion threshold ($\theta_d$) was set to $0.5 \times y_o^{snr}$, where $y_o^{snr}$ was the tonic level of GPi/SNr (Fig. 2(A)). In the time interval $t \leq 1$, the output reaches its 'default' or 'equilibrium' value which is the *tonic value* of the GPi/SNr (Fig. 2(A)). We further define time intervals 1 and 2 as $1 \leq t \leq 2$ and $2 \leq t$ respectively. We consider the two channel outputs during these intervals as $y_1^{snr}(1)$ and $y_2^{snr}(2)$. At time $t = 1$, channel 1 salience c1 increases from 0 to 0.4 (*shown in blue*, Fig. 2(A)). This induces a selection of channel 1 and an increase in $y_2^{snr}(2)$. At time $t = 2$, channel 2 increases its salience to 0.7 (*shown in red*, Fig. 2(B)). This induces a selection of channel 2, and a clear deselection of channel 1 (since now, $y_1^{snr}(1) > \theta_d$, Fig. 2(B)). This particular outcome is called *Switching* (See description below). However, this dual threshold scheme and pairwise competition between two channels could result in several outcomes — *conditions of selectivity*, which are detailed below.

#### 2.7.2. Conditions of selectivity

The six possible conditions of selectivity are described here (see also Gurney et al., 2004). They are the basic criteria used to classify selection possibilities. If $\wedge$ stands for conjunction then,

1. *No Selection* No channel selected: $[y_1^{snr}(1) > \theta_s] \wedge [y_1^{snr}(2) > \theta_s] \wedge [y_2^{snr}(2) > \theta_s]$
2. *Single Channel Selection*: Each interval has a clear single channel selected with no interference, distortion or switching. Two possibilities:
    - Channel 1 selected: $[y_1^{snr}(1) \leq \theta_s] \wedge [y_1^{snr}(2) \leq \theta_s] \wedge [y_2^{snr}(2) > \theta_s] \wedge [y_2^{snr}(2) > \theta_d]$

- Channel 2 selected: $[y_1^{snr}(1) > \theta_s] \wedge [y_1^{snr}(2) > \theta_s] \wedge [y_2^{snr}(2) \leq \theta_s] \wedge [y_1^{snr}(2) > \theta_d]$

3. *Switching*: Channel 2 is selected while channel 1 is deselected after being selected first, with no interference: $[y_1^{snr}(1) \leq \theta_s] \wedge [y_1^{snr}(2) > \theta_s] \wedge [y_2^{snr}(2) \leq \theta_s] \wedge [y_1^{snr}(2) > \theta_d]$
4. *Dual Channel Selection*: Channel 1 is selected in interval 1 and both channels are selected in interval 2:$[y_1^{snr}(1) \leq \theta_s] \wedge [y_1^{snr}(2) \leq \theta_s] \wedge [y_2^{snr}(2) \leq \theta_s]$
5. *Interference*: Channel 1 selected in interval 1. Channel 2 causes deselection of channel 1 in interval 2, while it does not itself become selected: $[y_1^{snr}(1) \leq \theta_s] \wedge [y_1^{snr}(2) > \theta_s] \wedge [y_2^{snr}(2) > \theta_s]$
6. *Distortion*: Single channel may be selected or switching might occur, the difference being that the losing channel is not clearly deselected, i.e, it is less than $\theta_d$. Three possibilities:

   - Channel 1 selected: $[y_1^{snr}(1) \leq \theta_s] \wedge [y_1^{snr}(2) \leq \theta_s] \wedge [y_2^{snr}(2) > \theta_s] \wedge [y_2^{snr}(2) \leq \theta_d]$
   - Channel 2 selected: $[y_1^{snr}(1) > \theta_s] \wedge [y_1^{snr}(2) > \theta_s] \wedge [y_2^{snr}(2) \leq \theta_s] \wedge [y_1^{snr}(2) \leq \theta_d]$
   - Switching: $[y_1^{snr}(1) \leq \theta_s] \wedge [y_1^{snr}(2) > \theta_s] \wedge [y_2^{snr}(2) \leq \theta_s] \wedge [y_1^{snr}(2) \leq \theta_d]$.

#### 2.7.3. Hard and soft selection through template matching

The salience on the two competing channels was varied from 0 to 1 in steps of 0.1, totalling 121 outcomes. We then observed which condition of selectivity, the pattern of outputs defined, for each salience pairing. This was done for a fixed value of dopamine ratio. In the GPR model, it was shown that for moderate levels of dopamine ($R_w = 1.83$) the outcomes favour *hard selection*, which is dominated by single-channel selection (Gurney et al., 2004, 2001a). Hard selection, was more crucial for a system working as a selection mechanism, as it was defined on the basis of a clear winner amongst competing channels. An ideal selection mechanism would normally require that there be a clear 'winner' of the competition for behavioural expression, facilitated by intermediate levels of dopamine. At sufficiently low levels of dopamine ($R_w = 1$) there is failure to select (See Figs. 3(C), 5(A) & (B)). This is consistent with the pathology of Parkinson's disease in which low levels of dopamine (typically more than 80% loss, Roessner et al. 2011; Yoon, Gause, Leckman, and Singer 2007) cause akinesia, which we interpret as a failure of action selection.

However, it may be desirable in some circumstances, that selection be more 'promiscuous' so that inhibition is removed from multiple channels. We refer to this as *soft selection* which consists largely of dual channel selection in the template description. Soft selection is favoured at higher levels of dopamine ($R_w = 10$). In its extreme form, such selection may be associated with undesired expression of actions simultaneously (or near simultaneous) with the desired, as shown, for example, in Tourette's syndrome, where undesirable behavioural 'tics' accompany normal target behaviours (Roessner et al., 2011; Yoon et al., 2007). However, there are other, more positive ways of interpreting soft selection and the nominal simultaneity of selection, which we discuss below.

#### 2.7.4. Understanding behavioural correlates of soft selection

Consider a model situation with dual channel selection. This is maintained in the model only via the artefact of sustained application of fixed input saliences on the relevant channels. In reality, if we close the environment-agent loop, the very act of committing an action by the agent will modify the agents perceived environment, thereby facilitating a change in salience which, in turn, may release any dual channel deadlock. This will also be assisted by any neural noise which we have omitted in the current model for simplicity. In either case, the final selection after this 'symmetry breaking' will be somewhat randomly obtained, and contingent on small phasic disturbances in the agent or its dynamically evolving environment. This kind of non-determinism in salience input will force the agent to *explore* a variety of actions in response to a general environmental context, as required, if the agent is to undergo effective reinforcement learning (Barto, 1994; Barto & Mahadevan, 2003). In our model, soft selection is favoured by higher levels of dopamine, indicating more exploratory behaviour under these conditions. This is consistent with some interpretations of the biological implications of increased dopamine; for example, increased activity in the dopamine system has been associated with higher levels of 'risk' taking during adolescence in human development (Wahlstrom, Collins, White, & Luciana, 2010). Furthermore, modelling suggests that low to moderate levels of tonic dopamine activity in the striatum induces *exploratory* behaviours (Chakravarthy & Balasubramani, 2013; Humphries, Khamassi, & Gurney, 2012), while higher levels induce exploitive or 'Go' behaviours (Frank, 2006)

While the 'symmetry breaking' account of soft selection may apply to a single competitive loop in the basal ganglia (the target of our model), soft selection may occur more generally in the wider context of multiple, parallel (and competitively more independent) loops. Parallel loops have been proposed in the basal ganglia for automatic and voluntary behaviours (Kim & Hikosaka, 2015). These can mediate behaviours which can and do occur simultaneously, in reward-seeking behaviours — as for instance eating and reaching out for food. This would mean disinhibition of different pattern generator circuits devoted to specific types of movements (Grillner et al., 1998). The basal ganglia output nuclei target all these motor generating circuits (Grillner, 2003; Grillner, Hellgren, Ménard, Saitoh, & Wikström, 2005; Kim & Hikosaka, 2015).

#### 2.7.5. Quantifying selection

We quantify selection outcomes by comparing the degree of match of our own experimental outcomes with 'ideal' templates for both hard and soft selection. The candidate templates we used for these comparisons are shown in Fig. 3(A) (hard selection) and Fig. 3(B) (soft selection, see also Gurney et al. 2004, 2001a). We thus used the comparison parameters, *Hard selection match* $P_h$, and the *Soft selection match* $P_s$ as,

$$P_h = \frac{N_h 100}{N}, P_s = \frac{N_s 100}{N} \tag{4}$$

where $N_h$ and $N_s$ were the salience value pairs for which the simulation outcomes matched their counterparts in the ideal hard and soft selection templates respectively, and $N$, the total number of salience value pairs. By repeating the 121 experiments in the 'salience grid' with several values of $\lambda$ ($0 < \lambda < 1$), we measured the $P_h$ and $P_s$ values across dopamine levels and plotted them against $R_w$. The points were fit using a cubic spline and the maximum $P_h$ and $P_s$ (Max $P_h$, Max $P_s$, peak of the corresponding spline, see Fig. 3(C)) were calculated. The value of the dopamine ratio at which the $P_{h(R_w)}$ and $P_{s(R_w)}$ trajectories cross was defined as the *Cross-over point* $W_c$ (Fig. 3(C)).

The general metric was to compare $P_h$ and $P_s$ values of our models with the corresponding values of the best performance simulation of the GPR model (Gurney et al., 2001b). We defined performance from a computational perspective based on the *ability* of the selection mechanism to perform better hard selection. Thus, an increase in Max $P_h$ compared to the Max $P_h$ of the GPR model (65.22, Fig. 3(C), Gurney et al. 2004, 2001a) was taken to be a performance increment. However, the selection system was also required to demonstrate large values of $P_s$ similar to the GPR model, ensuring sufficient access to both hard and soft selection regimes. We thus took minimal deviation of the Max $P_s$ value, or an increase

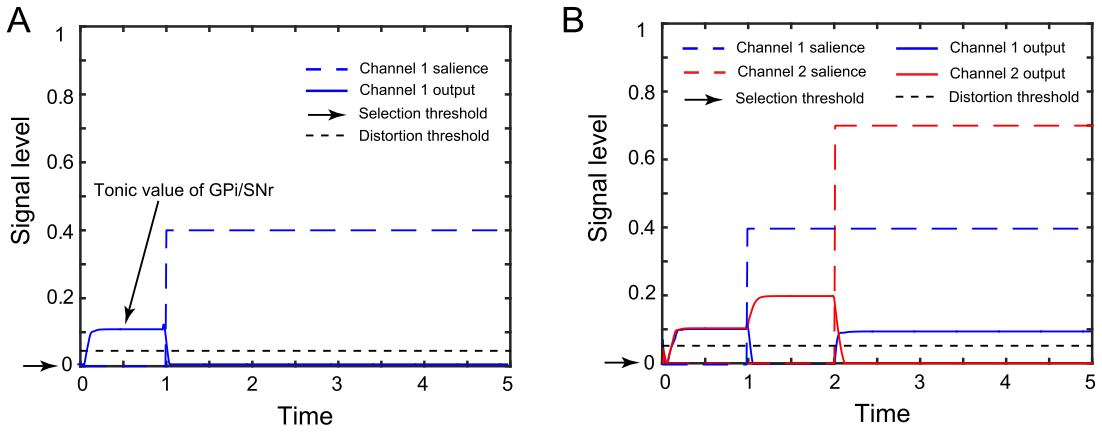


**Fig. 2.** *Experimental protocol with pairwise competition.* Description of the basic selection procedure **(A)** Channel 1 salience is increased to 0.4 which leads to its selection at$t = 1$ **(B)** Channel 2 salience is then increased to 0.7 at $t = 2$, which leads to its selection and a clear deselection of channel 1, a condition of selectivity called 'switching'. Note that the output of channel 1 at $t = 2$, is above the distortion threshold ($\theta_d$) indicating its clear deselection. (For interpretation of the references to colour in this figure legend, the reader is referred to the web version of this article.)

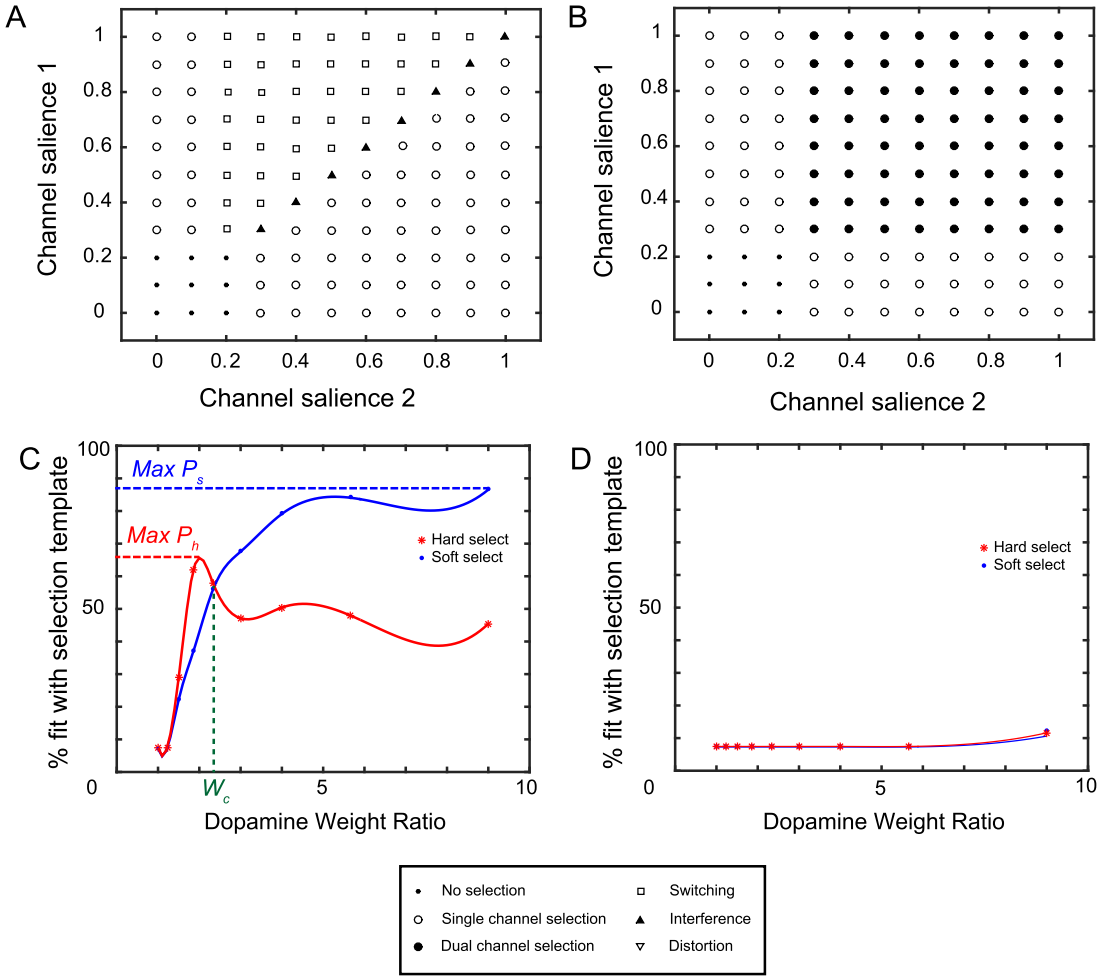


**Fig. 3.** *Selection templates and performance trajectories.* **(A)** Ideal *Hard* and **(B)** *Soft* selection templates used for comparisons of our simulation outcomes. **(C)** Hard and soft trajectories across dopamine range, of the best performance of the GPR model, which highlights the desirable trajectories of $P_h$ and $P_s$, each having high values and sufficient difference between them. The values are Max $P_h = 65.22$, Max $P_s = 86.78$ and the cross-over point $W_c = 2.35$ **(D)** shows a model run with a biologically implausible weight from one of our step-wise models, indicates the failure of the model-the hard and soft curves nearly overlap. The curves are cubic spline fits to data. (For interpretation of the references to colour in this figure legend, the reader is referred to the web version of this article.)

from that of the GPR model (86.78, Fig. 3(C)) as another indicator of model performance.

We also evaluated the general trajectories of both $P_h$ and $P_s$ plots across $R_w$ in terms of their resemblance to what was seen in the GPR model (Fig. 3(C)). In general, the $P_h$ trajectory $>$ $P_s$ for low dopamine, must cross each other subsequently at a point defined as the crossover-point $W_c$, and for higher dopamine value, $P_s$ trajectory $>$ $P_h$. This translates to the function $P_h(R_w)$ increasing

from $P_h(1)$, reaching its peak Max $P_h$ at relatively small values of $R_w$ and then decreasing gradually with increase in $R_w$. The function $P_s(R_w)$ on the other hand, increased monotonically from $P_s(1)$, reaching the peak value Max $P_s$ at large values of $R_w$. The cross-over point $W_c$ essentially determined that for $1 < R_w < W_c$, $P_h > P_s$ the system was in the *hard selection regime*. For $R_w > W_c$, $P_s > P_h$ the system was in the *soft selection regime*. Thus, there had to be a clear distinction and difference between the fits of $P_h$ and $P_s$ across $R_w$, and any overlap was considered as a failure of the model (Fig. 3(D), See also Gurney et al. 2004). This was important in that it forced a clear distinction in the models behaviour in terms of hard and soft selection. The cross-over point in addition, also determined the range of dopamine values through which hard selection may be accessed by the model, and its value being equal to or greater than that of the GPR model (2.35, Fig. 3(C)), was also an additional determinant of model performance.

Each of the three parameters defined — Max $P_h$, Max $P_s$ and $W_c$, represented a feature of the model and contributed in its own right towards the assessment of the performance of the model. We thus had the feature set F = {Max $P_h$, Max $P_s$, $W_c$}. However, the basis of our performance metric was changes of performance in relation to that of the GPR model. We therefore defined these features relative to those of the GPR model as $R_i = log(r_i)$, where $r_i = f_i/f_{GPR}$ with $f_i \in$ F, and where $f_{GPR}$ was the value of the corresponding feature in the GPR model. This resulted in the defining of relative features to the three features F = {Max $P_h$, Max $P_s$, $W_c$} as $\{R_i\} = \{H^*_{MAX}, S^*_{MAX}, W^*_c\}$ respectively. Bringing these ideas together allows us to define a single scalar metric $Q^*$ which added up the three relative features as,

$$Q^* = \sum_i log(r_i). \tag{5}$$

Thus, an increase in $Q^*$ following any addition of a biologically plausible pathway to the GPR model would indicate an increment in performance, implying greater support for the action selection hypothesis.

#### 2.7.6. Reversal phenomenon

In the extended architecture simulated in this study, we observed a hitherto unseen 'reversing' of tendency of a particular channel to get selected, with increasing salience. In general, as the salience is increased for a particular channel, its output decreases and approaches the selection threshold (which is zero). However, in some models with newly included pathways here, it was observed that across a range of high salience values, with increasing salience values, when the salience on one channel was kept constant and that on the second increased, the output of the latter channel increased, rather than decrease (and thereby approach the selection threshold) *reversing* the tendency to get selected. We defined a value to quantify this phenomenon — a *Reversal* $R_v$ which was given by,

$$R_v = \frac{N_r 100}{N} \tag{6}$$

where $N_r$ was the number of channel 1 and channel 2 salience value pairs for which reversal occurs and $N$ the total number of salience value pairs (within the experimental 'salience grid' defined previously). This unitary phenomenon (increase in output with increased salience), resulted in four possible cases: *Single Ch selection → No Selection, Dual channel selection → Interference/Distortion/Switching, Switching → Interference/Distortion and Distortion → Interference*. Some of these cases are illustrated in Fig. 4. These various cases were seen in control models of pathways underlying reversal (see reversal architecture, Fig. 10(B)). In the final model, only the cases resulting in Dual channel selection → Interference/Distortion/Switching, were seen, largely in the soft selection regime (see Fig. 7(F) and Discussion). We do not detail the types of reversal in different models, but present its occurrence in terms of Reversal value defined here.

Thus, mechanistically, reversal by large, enables soft selection outcomes (dual channel selection) being reversed to hard selection outcomes (single channel outcomes). Since reversal occurred across a range of high salience values, we speculate that it may be indicative of exploratory behaviours (Chakravarthy & Balasubramani, 2013; Humphries et al., 2012) but also resolution of 'flight-fight' instances of behavioural decision-making.

#### 2.7.7. Other features

As well as determining the values of metrics such as $Q^*$ and $R_v$, we also report a range of features about model behaviour, such as presence or absence of oscillations, changes in tonic rates of the GPi/SNr. We also attempt to dissect out neural connectivity underlying some of these features and identify the roles of different pathways in these features, which are tabulated in Table 4.

### 2.8. Extended architecture — omissions

The extended architecture incorporates most of the neural subpopulations and intrinsic connectivity of the GPe known. However, not all logically possible pathways are investigated as we had to limit the combinatorics to be tractable. The rationale for omissions is as follows: The projections from SPN D1 neurons to GPe TI and GPe TA have been omitted, since their primary role is in relation to the direct pathway. With respect to the projections of the GPe TA neurons to the striatum, we have modelled only the projections to the SPNs. The extent and distribution of the GPe TA neuronal projections to the striatum is not yet completely clear, although they are known to target both the SPNs and the interneurons (Burke, Rotstein, & Alvarez, 2017; Hegeman et al., 2016; Mallet et al., 2012). Furthermore, there are some indications that GPe TA input to D2 SPNs is stronger (Glajch et al., 2016), however, we have not varied the relative strengths of GPe TA projections to D1 and D2 SPNs. We have also not modelled the GPe TA local collaterals to the GPe TI, whereas the reverse connection has been included. There is recent evidence from modelling that GPe TA neurons receive inputs from the GPe TI (Lindahl & Hellgren Kotaleski, 2016), which agrees with our own modelled connectivity. The final form of the new extended architecture is seen in Fig. 1(D). The TI and TA neurons are shown within the GPe boundary, whereas the outer and inner neurons are shown within the TI boundary. The extrinsic connections of both the outer and inner neurons are commonly represented by the TI, except for the distinguishing connection between the outer and inner neurons.

## 3. Results

Recall from the methods that we make use of step-wise and combined models, investigating single and multiple pathways respectively, and that their deployment is carried out in three modelling phases. This approach is reflected here in reporting the Results.

### 3.1. Phase 1: TA step-wise models

In phase 1, the GPe TA neurons were added to the GPR model. The results of each of the step-wise models are described below. The different weights used in each of the step-wise models are tabulated in Appendix S2.

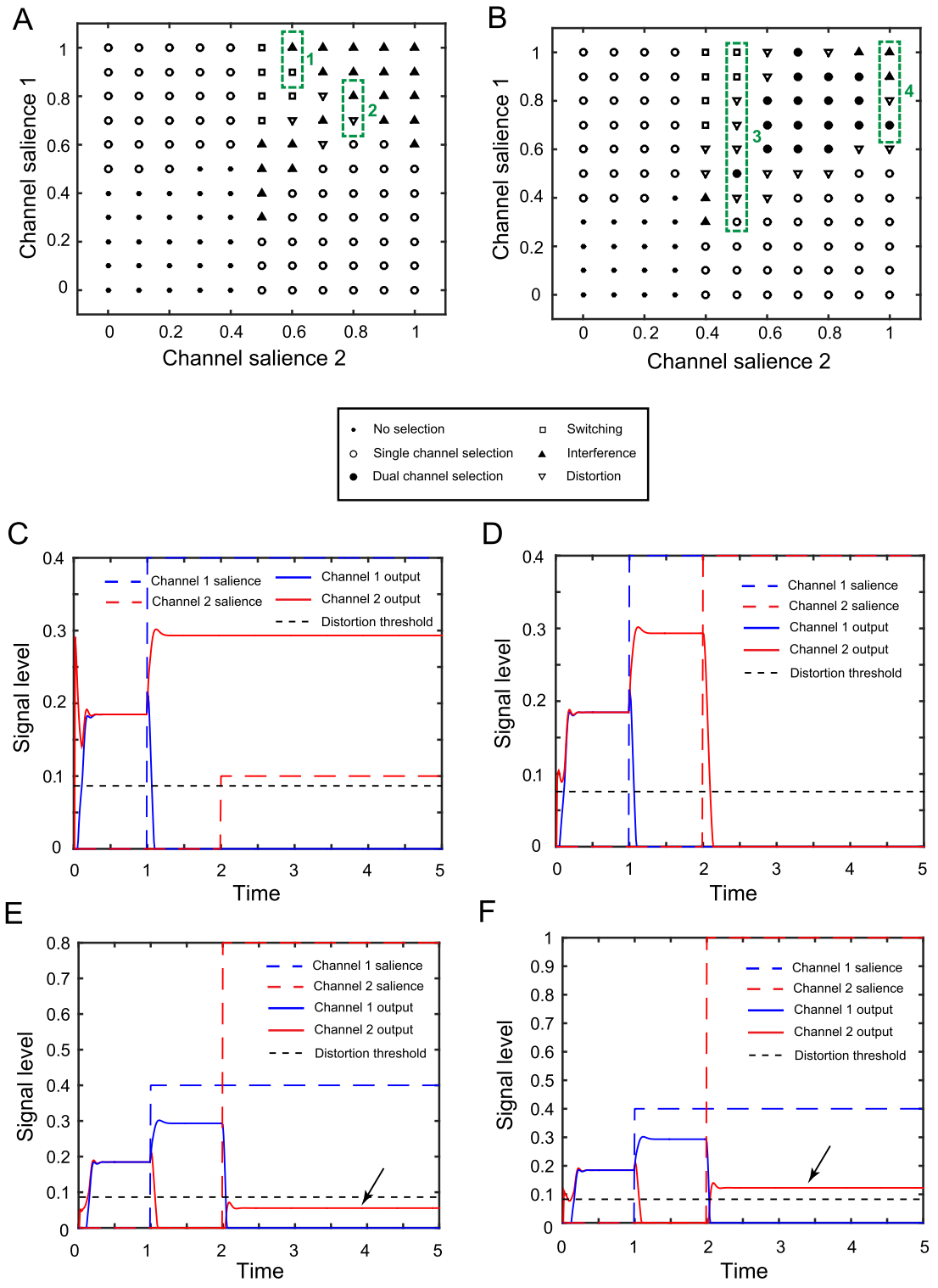


**Fig. 4.** *Reversal phenomenon.* Reversal seen here on the selection outcomes from **(A)** one of the control models (**1,2**, *green dotted box*) shows the case where after *switching* the selected channel is pulled back causing *interference*. In **(2)** *distortion* is followed by *interference* instead of the normal *switching*. These types of reversal cases were only seen in control models. **(B)** Reversal in the final model, in **(3)** *dual channel selection* is followed by *distortion* and *switching* while in **(4)** it is followed by *distortion* and *interference*. These cases aid in better action selection performance in that they lessen the number of more promiscuous selections. **(C-D)** Time course of a typical reversal case occurring in the final model as per the sequence seen in **(3)**, in **(C)** channel 1 is selected upon reaching the selection threshold, following which in **(D)** the salience of channel 2 increases sufficiently to result in its selection as well — *dual channel selection*. Reversal kicks in, and in **(E)** channel 2 output can be seen to increase (*black arrow*), causing *distortion* (its output is still lesser than the distortion threshold). Subsequently however in **(F)**, the channel 2 output increases above the distortion threshold, resulting in its clear deselection, resulting in *switching*. Thus reversal resulted in a reversion back to a clear selection of channel 1 from the scenario where both channel 1 & 2 were selected. (For interpretation of the references to colour in this figure legend, the reader is referred to the web version of this article.)

*3.1.1. GPe TA–GPe TA step-wise model*

This model tested the feedback pathways of the GPe TA neurons (pathway 1 in Fig. 1(B)). The feedback loop of the GPe TI $w^{-}_{ti-ti}$, was set to 0 to isolate the GPe TA–GPe TA pathway as much as possible. Only $w^{-}_{ta-ta}$ was varied. The projections to striatum, $w^{-}_{ta-d1}$ and $w^{-}_{ta-d2}$ were set at $-1$, while the $w^{-}_{ti-ta}$ was set at $-1$. $w^{-}_{ta-ta}$ had no effect on $P_h$ or $P_s$, as it was varied. $H^*_{MAX}$ and $W^*_c$ were slightly higher than the GPR values while $S^*_{MAX}$ was unchanged. The performance $Q^*$ was only slightly higher than the GPR model (Fig. 6(A)–(D)). There was no change in tonic level of GPi/SNr. This pathway has no significant influence on selection as the $P_{h(R_w)}$ and $P_{s(R_w)}$ trajectories were similar to that of the GPR model (Fig. S1 A). Reversal was also not noticed; this path had no role in reversal phenomenon. The model produced oscillations, and in order to find the source of oscillations more precisely, $w^{-}_{ta-d1}$ and $w^{-}_{ta-d2}$ were varied. It was found that oscillations were sustained for $w^{-}_{ta-d1} = w^{-}_{ta-d2} = -1$, indicating that both the arkypallido-striatal components were required to generate them (see Table 4). Oscillations were sustained at lower DA levels and were maximum when there was no dopamine activity (DA = 0, Fig. 5(A)). They reduced in amplitude as DA level increased DA $\leq$ 0.3 (Fig. 5(B) & (C)), and were completely suppressed for DA $\geq$ 0.4 (Fig. 5(D)). The oscillations had a frequency of 4.7 Hz and were therefore classified as being in the theta band. Furthermore, for DA = 0, the outputs at the level of GPe subpopulations and STN were also evaluated. Both the GPe subpopulations — arkypallidal and prototypical neurons were oscillating (Fig. 5(G)) as well as STN (Fig. 5(H)). Thus the entire STN–GPe–GPi/SNr network oscillates.

*STN stimulation.* We checked whether over activation of the STN in the model conditions which produced oscillations, could relieve oscillations. All the weights associated with the STN were set to +1 to capture the conditions of STN stimulation. The model performance was tested for DA = 0 and the model was able to select and the oscillations were suppressed (Fig. 5(G), see also Fig. S4B & D, for weights of different pathways see 'STN–DBS model' in Appendix S2). The Max $P_h$ value was higher than the oscillating condition (Fig. S4D).

*STN lesion.* We furthermore checked whether lesioning of STN could provide similar outcomes — in this case all the weights associated with STN were set to 0). Interestingly, for DA = 0, the model was able to select as well as suppress oscillations (Fig. 5(H), see also Fig. S4C & D, for weights of different pathways see 'STN-lesion model' in Appendix S2).The Max $P_h$ value was higher than the oscillating condition (Fig. S4D).

*3.1.2. GPe TA–STR step-wise model*

This model tests the diffuse projections of the GPe TA neurons to the striatum (pathway 2 in Fig. 1(B)). The weights $w^{-}_{ta-d1}$ and $w^{-}_{ta-d2}$ were varied but were kept equal. The GPe TI–GPe TA pathway weight $w^{-}_{ti-ta}$ was also varied. GPe TI was necessary since the GPe TA neurons have no efferents to the GPi/SNr. To test the pathways in as much isolation as possible, the feedback weights of GPe TI and GPe TA neural populations were 'lesioned', $w^{-}_{ti-ti} = w^{-}_{ta-ta} = 0$. $H^*_{MAX}$ was lower than the GPR value showing this projection reduced the performance of the model in the hardness regime. However, with increase in $W^*_c$, it increased the range of the hardness regime across dopamine values. $S^*_{MAX}$ was also reduced. The performance $Q^*$ was higher than the GPR model, largely due to the marked increase of $W^*_c$ (Fig. 6(A)–(D)). Oscillations were observed for $w^{-}_{ti-ta} = -1$ and $w^{-}_{ta-d1} = w^{-}_{ta-d2} = -1$, just as they were observed in the GPe TA–GPe TA step-wise model. It was confirmed that these pathways were responsible for oscillations (see Table 4). The dependence of oscillations on low dopamine levels was also confirmed. Even for the values of best performance, $w^{-}_{ti-ta} = -0.75$ and $w^{-}_{ta-d1} = w^{-}_{ta-d2} = -0.25$, the $P_{h(R_w)}$ and $P_{s(R_w)}$ trajectories overlapped (Fig. S1B). This was a failure of the model — indicating that the connectivity was incomplete and not fit for optimum action selection. Reversal was not observed indicating that these pathways had no role in reversal phenomenon.

*GPe TI–TA step-wise model*

This model tested the GPe TI–GPe TA pathway $w^{-}_{ti-ta}$, which was added to the GPR model (pathway 3 in Fig. 1(B)). This would be analogous to the GP-outer to GP-TA connection in future models. Both $w^{-}_{ti-ti}$ and $w^{-}_{ta-ta}$ were set to 0 or 'lesioned' to provide for exclusive testing. The TA projections to the striatum, $w^{-}_{ta-d1}$ and $w^{-}_{ta-d2}$ were set to $-1$. $H^*_{MAX}$ was higher the GPR value which resulted in the performance $Q^*$ being slightly higher than the GPR. $S^*_{MAX}$ and $W^*_c$ were unchanged (Fig. 6(A)–(D)). The model showed no selection till $w^{-}_{ti-ta} = -0.75$, and selection was observed at $w^{-}_{ti-ta} = -1$ (Fig. S1C). There was no influence on the GPi/SNr tonic level or any significant influence on selection. There was no role of this pathway in reversal, which was not noticed. This pathway allows the prototypical TI neurons to maintain control on the arkypallidal TA neurons, inturn allowing them to influence striatal activity (see Table 4).

*3.1.3. GPe TI–TI step-wise model*

This model tested the local inhibitory connections of GPe TI neurons, considered as a single homologous population (pathway 4 in Fig. 1(B), analogous also to pathway *, GPe outer–GPe outer in Fig. 1(C)). This did not include the GPe TA neurons or the outer/inner neuron distinction of GPe TI neurons. The GPe TI–SNr weight was fixed at $w^{-}_{ti-snr} = -0.4$. The GPe TI–GPe TI feedback weight, $w^{-}_{ti-ti}$ was varied. Both $H^*_{MAX}$ and $S^*_{MAX}$ were reduced, however $W^*_c$ was increased which yielded in an increased performance $Q^*$ than the GPR model (Fig. 6(A)–(D)). Max $P_h$ occurred for $w^{-}_{ti-ti} = 0$, which was the same as the GPR model. Clearly this pathway was, at this stage not useful for action selection. This indicated lack of sufficient circuitry modelled. We have, however, shown the simulation result with $w^{-}_{ti-ti} = -0.25$ (Fig. S1D), which was the weight of this pathway, for best performance in the final model (see below). Reversal was observed for $w^{-}_{ti-ti} > 0$ (see Fig. 7(A)) showing that the TI neurons play a role in reversal. Tonic value of GPi/SNr increased with increase in $w^{-}_{ti-ti}$ (see Fig. 8(A) and Table 4). The pathway thus influences selection by setting the tonic value of GPi/SNr.

*3.2. Phase 2: TI step-wise models*

In phase 2, the GPe TI neurons with the outer–inner dichotomy were added to the GPR model. The results of each of the step-wise models are described below. The different weights used in each of the step-wise models are tabulated in Appendix S2.

*3.2.1. GP IN–GP IN step-wise model*

This was the first model incorporating the dichotomy of GPe TI neural population — the outer and inner neurons. The GPe TI–GPe TI step-wise model was equivalent to GPe outer–GPe outer step-wise model, so we start from investigating the GPe inner–GPe inner step-wise model (pathway 5 in Fig. 1(C)). To investigate this pathway exclusively, we set the GPe outer–GPe outer (TI–TI) weight, $w^{-}_{ot-ot} = -1$ and the GPe outer–GPe inner weight $w^{-}_{ot-in} = -1$, and varied $w^{-}_{in-in}$. We also 'lesioned' the GPe outer–SNr pathway $w^{-}_{ot-snr} = 0$, so as to have only the output of GPe inner neurons to the GPi/SNr. Both $H^*_{MAX}$ and $S^*_{MAX}$ were reduced, however $W^*_c$ was increased which yielded in an increased performance $Q^*$ than the GPR model (Fig. 6(A)–(D)), similar to the GPe TI–GPe TI model, indicating these two pathways may be involved in similar functions. Reversal was noticed, even when $w^{-}_{ot-ot} = 0$ (Fig. 7(B)) indicating this pathway and by extension — the inner neuron play

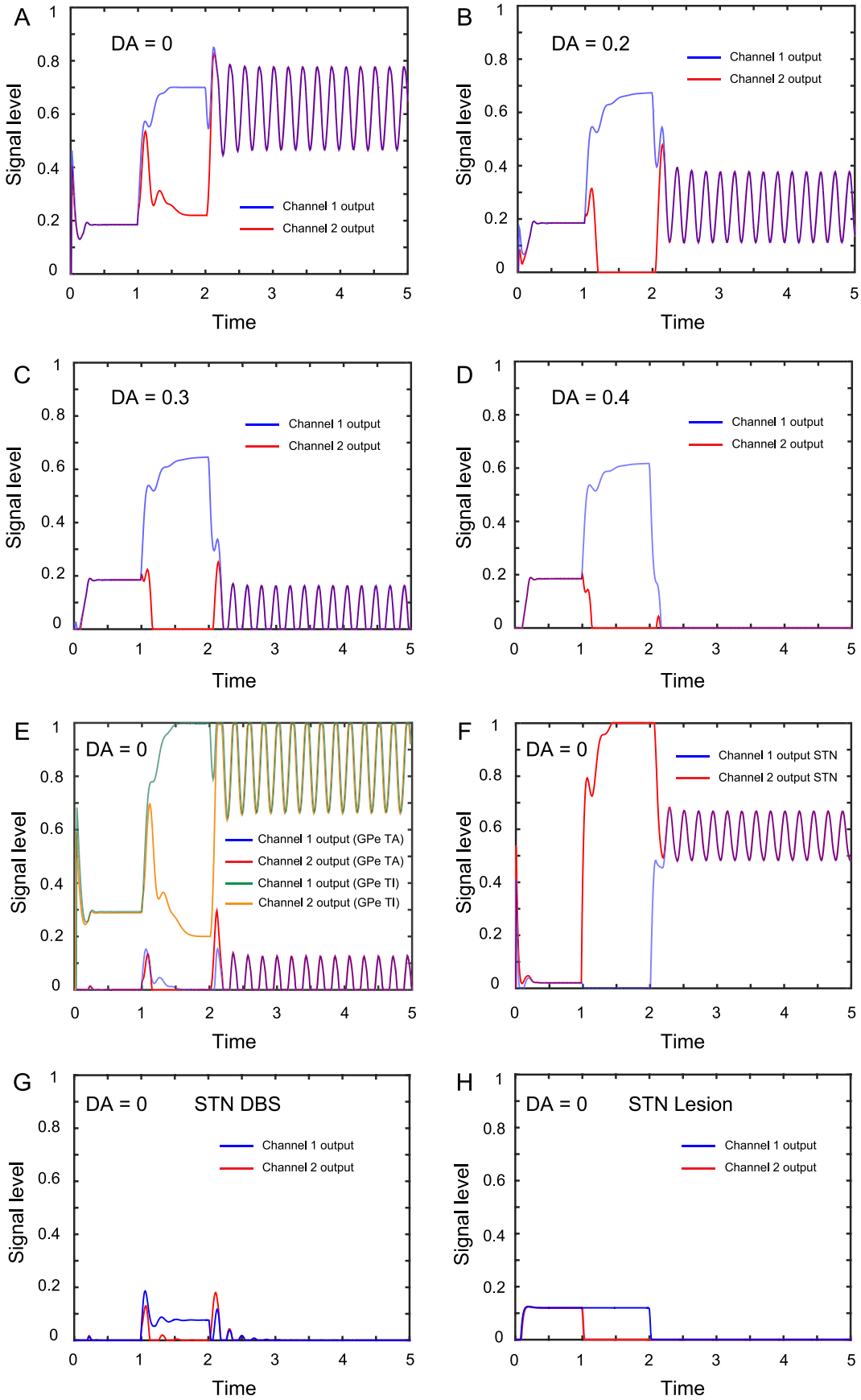


**Fig. 5.** *Theta oscillations induced by lack of dopamine.* Oscillations across dopamine levels, Max Amplitude at **(A)** DA = 0, Intermediate levels **(B)** DA = 0.2 and **(C)** DA = 0.3, Suppressed at **(D)** DA = 0.4. The oscillations were due to the arkypallidal TA projections to the striatum. **(E)** Oscillations at DA = 0, also at the level of GPe subpopulations — both the arkypallidal and prototypical neurons. **(F)** Oscillations also at the level of STN for DA = 0. **(G)** Suppression of oscillations and selection induced for DA = 0 for maximum weights on STN mimicking STN — deep brain stimulation conditions. **(H)** Similar suppression of oscillations and selection when STN weights are made zero reflecting 'STN-lesion' condition. (For interpretation of the references to colour in this figure legend, the reader is referred to the web version of this article.)

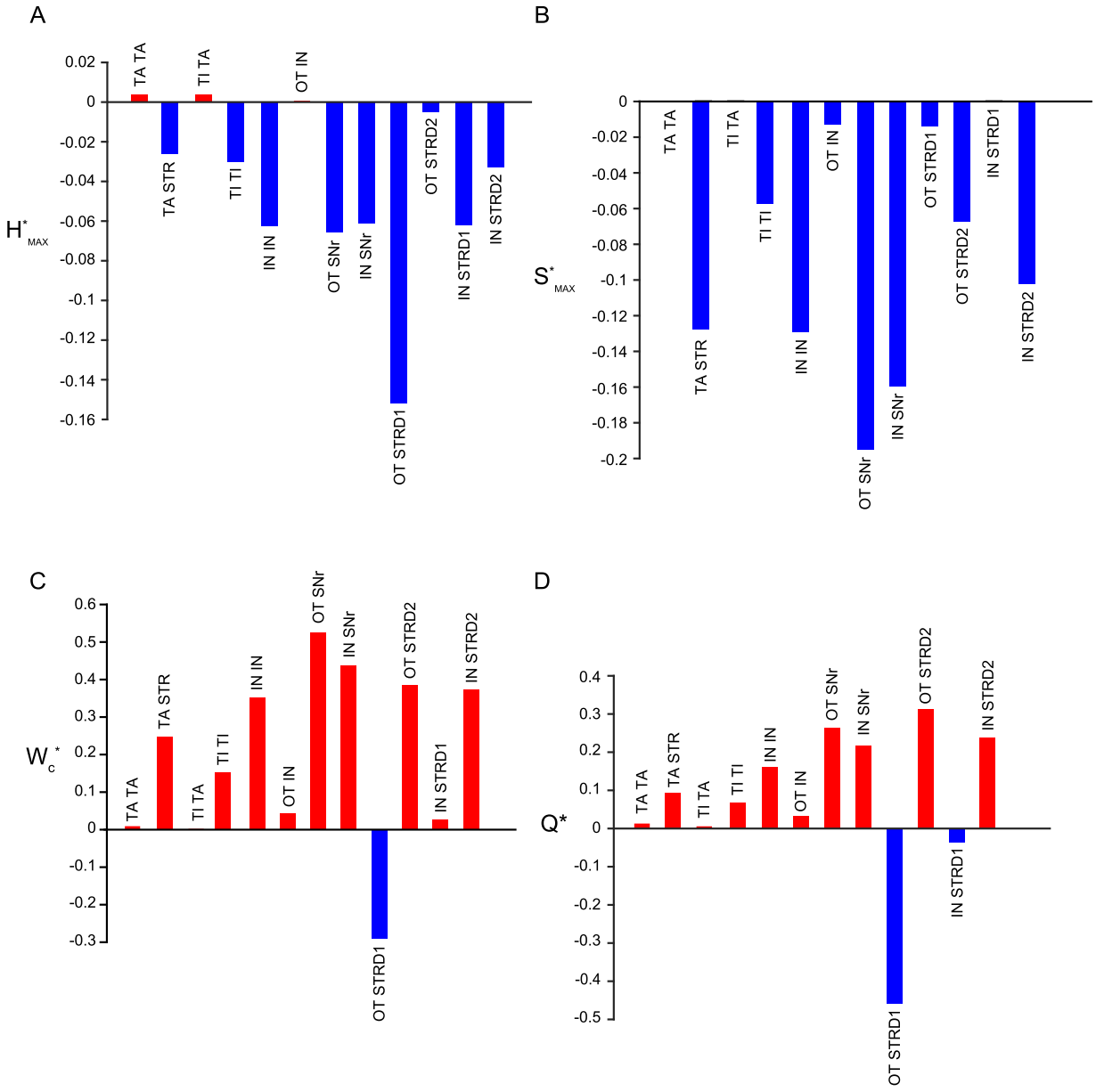


**Fig. 6.** *Performance metrics.* Performance metrics for the step-wise models **(A)** $H^*_{MAX}$ values showing the relative change in Hard selection of the step-wise models to that of the GPR model **(B)** $S^*_{MAX}$ values showing the relative change in Soft selection of the step-wise models to that of the GPR model **(C)** $W^*_c$ values showing the relative change in cross-over point of the step-wise models to that of the GPR model **(D)** $Q^*$ Performance metric values of step-wise models relative to the GPR model. In all, red plots indicate increment in value while blue plots indicate decrement in value. (For interpretation of the references to colour in this figure legend, the reader is referred to the web version of this article.)

a role in generating reversal (see Table 4). Tonic value of GPi/SNr increased with increase in $w^-_{in-in}$ (Fig. 8(A)) also implicating the inner neurons in influencing the tonic output of the GPi/SNr (see Table 4). Max $P_h$ occurred for $w^-_{in-in} = -0.5$. However, there was a near overlap of $P_{h(R_w)}$ and $P_{s(R_w)}$ trajectories, which was clearly undesirable (Fig. S1E) and indicated incomplete connectivity. In the final model (see below) a weight of $w^-_{in-in} = -0.75$ was used, which yielded best performance.

### 3.2.2. GP OT–GP IN step-wise model

This model investigated the crucial GPe outer–GPe inner link, which was the inhibitory connection between the GPe outer and GPe inner neuron populations (pathway 6 in Fig. 1(C)). $w^-_{ot-in}$ was varied, whereas same population inhibitory connection weights were set to, $w^-_{ot-ot} = w^-_{in-in} = -1$. $H^*_{MAX}$ was unchanged from that of the GPR model, while $S^*_{MAX}$ was reduced. $W^*_c$ was increased which yielded in an increased performance $Q^*$ (Fig. 6(A)–(D)). When $w^-_{ot-in} = 0$, the model behaved like the GPR model, which was also the best performance (Fig. S1F). However we used a value of $w^-_{ot-in} = -0.25$ in the final model, which gave best performance, which we have shown here as well. Reversal was noticed across the values of $w^-_{ot-in}$ (Fig. 7(C)). However, when the same population inhibitory weights were 'lesioned', i.e, $w^-_{ot-ot} = w^-_{in-in} = 0$, no reversal was noticed. Thus, this pathway had no role in generating reversal. Tonic level of GPi/SNr increased with increase in $w^-_{ot-in}$ (see Fig. 8(A) and Table 4).

### 3.2.3. GP OT–SNr step-wise model

This model investigated the efferents of the GPe outer neurons to the GPi/SNr (part of pathway 7 in Fig. 1(C), considering only GPe outer). The same population inhibitory weight was set at $w^-_{ot-ot} = -1$. The GPe outer–SNr weight $w^-_{ot-snr}$ was varied. Both

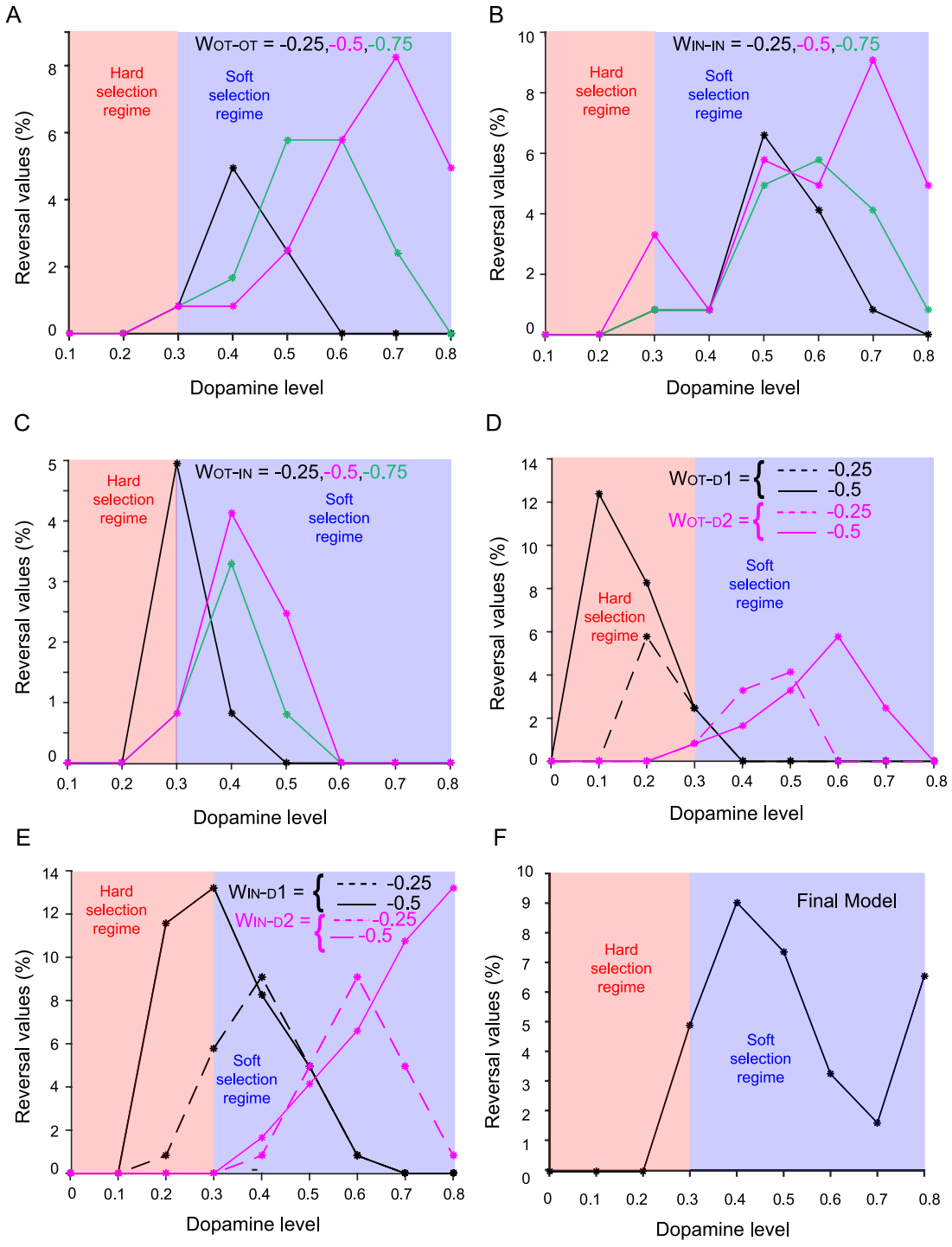


**Fig. 7.** *Reversal phenomenon generated by prototypical GPe neurons.* Reversal (in %) across dopamine levels and Hard and Soft selection regimes, with change in the weights of **(A)** $w^{-}_{ot-ot}$ (**(B)** $w^{-}_{in-in}$ **(C)** $w^{-}_{ot-in}$ **(D)** $w^{-}_{ot-d1}$&$w^{-}_{ot-d2}$ **(E)** $w^{-}_{in-d1}$&$w^{-}_{in-d2}$. **(F)** shows reversal observed in the final model across dopamine values, occurring largely in the soft selection regime. (For interpretation of the references to colour in this figure legend, the reader is referred to the web version of this article.)

$H^{*}_{MAX}$ and $S^{*}_{MAX}$ were reduced. $W^{*}_{c}$ was increased which resulted in an increased performance $Q^{*}$ (Fig. 6(A)–(D)). This pathway decreased the tonic level of GPi/SNr markedly with increase in $w^{-}_{ot-snr}$ (Fig. 8(B), see also Table 4). Clearly, this would facilitate selection, since a lower salience would be sufficient to ensure selection. Thus, the outer neurons made it easier for competing channels to be selected — *soft selectors* (Fig. 10(D), see Discussion). Although reversal was observed, this was due to the same population inhibitory weight being $w^{-}_{ot-ot} = -1$. When $w^{-}_{ot-ot} = 0$, no reversal was seen. Thus, this pathway does not generate reversal but executes it (see Table 4), as it is the pathway targeting the output nuclei. Best performance occurred for $w^{-}_{ot-snr} = -0.6$ (Fig. S2A), and Max $P_h$ increased with increasing $w^{-}_{ot-snr}$ till $-0.6$ and then decreased.

### 3.2.4. GP IN–SNr step-wise model

This model investigated the efferents of the GPe inner neurons to the SNr (part of pathway 7 in Fig. 1(C), considering only GPe inner). The same population inhibitory weight was set at $w^{-}_{in-in} = -1$ and that of GPe outer neurons $w^{-}_{ot-ot} = -1$ as well. The GPe outer–GPe inner weight was set at $w^{-}_{ot-in} = -1$. The GPe

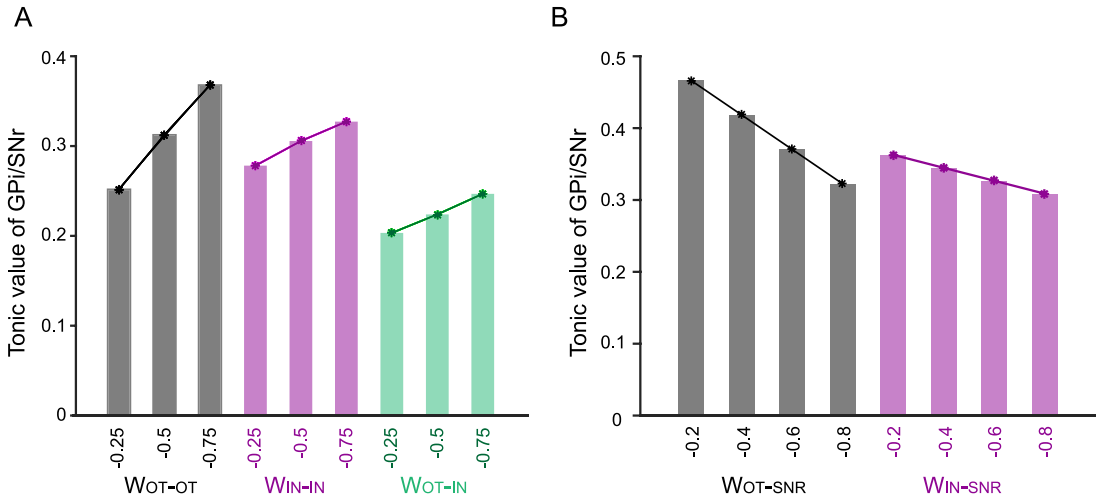


**Fig. 8.** *Effects of prototypical GPe neuron projections on tonic level of GPi/SNr.* Step changes in GPi/SNr tonic levels with change in the weights of (A) $w^{-}_{ot-ot}$ , $w^{-}_{in-in}$&$w^{-}_{ot-in}$ (B) $w^{-}_{ot-snr}$&$w^{-}_{in-snr}$. (For interpretation of the references to colour in this figure legend, the reader is referred to the web version of this article.)

inner–SNr weight $w^{-}_{in-snr}$, was varied. The GPe outer–SNr pathway was 'lesioned', $w^{-}_{ot-snr} = 0$, so as to enable examination of GPe inner–SNr pathway in isolation. Both $H^{*}_{MAX}$ and $S^{*}_{MAX}$ were reduced. $W^{*}_{c}$ was increased which resulted in an increased performance $Q^{*}$, the metrics resemble those of the GPe outer–SNr step-wise model (Fig. 6(A)–(D)). The tonic level of GPi/SNr, like with their GPe outer counterparts, decreased with increase in $w^{-}_{in-snr}$ (Fig. 8(B), see also Table 4), indicating similar roles for these pathways in setting the tonic level of GPi/SNr, although the decrease was lesser compared to the latter. Thus, the inner neurons made it less easier for channels to be selected, since they required higher salience in comparison to the outer neurons. This made the inner neurons — *hard selectors* (Fig. 10(D), see Discussion). Reversal was observed, even when both same population inhibitory pathways were set to $w^{-}_{ot-ot} = w^{-}_{in-in} = 0$. However GPe outer–GPe inner weight was high $w^{-}_{ot-in} = -1$. When $w^{-}_{ot-in} = 0$, reversal disappeared. Thus, this pathway had no role in generating reversal but executed it (see Table 4), just like its GPe outer–SNr counterpart. Best performance occurred for $w^{-}_{in-snr} = -0.6$ (Fig. S2B).

### 3.2.5. GP OT–STRD1 step-wise model

This model investigated the effect of the projections of GPe outer neurons to the striatum, in this case, striatum D1 (part of pathway 8 in Fig. 1(C), considering only GPe outer to STRD1). These projections were modelled as excitatory, since they innervate the FSNs in the striatum. This model investigates the effect on the selection pathway. We vary the weight $w^{+}_{ot-d1}$. The same population inhibitory weight was set to $w^{-}_{ot-ot} = 0$. All features, $H^{*}_{MAX}$, $S^{*}_{MAX}$ and $W^{*}_{c}$ showed a decrement in performance which consequently reduced $Q^{*}$ (Fig. 6(A)–(D)). This indicated that this pathway was not favourable for action selection. However, this was due to lack of more complete circuitry. Although best selection occurred for $w^{+}_{ot-d1} = 0$, we use a value of $w^{+}_{ot-d1} = 0.5$, which gave best performance in the final model (Fig. S2C). At a high weight, $w^{+}_{ot-d1} = 1$, at DA = 0, distortion and interference was noticed across saliences, while at high DA, dual channel selection across saliences was observed. Tonic level of GPi/SNr remained constant till $w^{+}_{ot-d1} = 0.5$ and then increased for subsequent higher weights. Clearly, high weights on this pathway were detrimental to action selection (see Discussion). Reversal was observed for DA $\leq$ 0.3, indicating its role in causing reversal in the hard selection regime (Fig. 7(D), see Table 4).

### 3.2.6. GP OT–STRD2 step-wise model

This model investigated the effect of the projections to the GPe outer neurons to the control pathway — striatum D2 (part of pathway 8 in Fig. 1(C), considering only GPe outer to STRD2). All the conditions of the previous model remained, except for the GPe outer projections to the selection pathway, which were 'lesioned' $w^{+}_{ot-d1} = 0$. $H^{*}_{MAX}$ and $S^{*}_{MAX}$ showed a decrement while $W^{*}_{c}$ showed a marked increase consequently improving performance $Q^{*}$ (Fig. 6(A)–(D)). This shows that this pathway is more favourable for action selection unlike its sister projections which affects striatum D1 SPNs (see Discussion). Reversal was noticed for $w^{-}_{ot-in} = -0.25$ and $w^{+}_{ot-d2} \leq 0.5$ and DA $\geq$ 0.3, indicating its role in causing reversal largely in the soft selection regime (Fig. 7(D), see Table 4).

### 3.2.7. GP IN–STRD1 step-wise model

This model investigated the projections of GPe inner neurons to striatum D1, to the selection pathway, which were modelled as excitatory due to their targeting FSNs (part of pathway 8 in Fig. 1(C), considering only GPe inner to STRD1).The weight of the GPe outer–GPe inner pathway, $w^{-}_{ot-in}$, was varied as well. The output of the GPe outer neurons was 'lesioned' $w^{-}_{ot-snr} = 0$, to isolate GPe inner output. $H^{*}_{MAX}$ and $S^{*}_{MAX}$ showed a marked decrement. Although $W^{*}_{c}$ showed a slight increase, there was a decrease of performance $Q^{*}$ (Fig. 6(A)–(D)). Again this is an undesirable pathway for action selection similar to GP OT–STRD1. The model had best performance for $w^{+}_{in-d1} = w^{-}_{ot-in} = 0$, equal to GPR model. However, we used weight of $w^{+}_{in-d1} = 0.25$ and $w^{-}_{ot-in} = -0.25$ (Fig. S2E) in the final model which yielded best performance. Tonic level of GPi/SNr remained constant till $w^{+}_{in-d1} = 0.5$ then decreased. Reversal was noticed for $w^{-}_{ot-in} = -0.25$ and $w^{+}_{in-d1} \leq 0.5$, and for DA $\leq$ 0.6 (Fig. 7(E)), indicating its role in causing reversal largely in the hard selection regime and at intermediate dopamine levels (see Table 4).

### 3.2.8. GP IN–STRD2 step-wise model

This model investigated the projections of GPe inner neurons to striatum D2, to the control pathway (part of pathway 8 in Fig. 1(C), considering only GPe inner to STRD2). The weight of the GPe outer–GPe inner pathway, $w^{-}_{ot-in}$, was varied as well. The output of the GPe outer neurons was 'lesioned' $w^{-}_{ot-snr} = 0$, to isolate GPe inner output. $H^{*}_{MAX}$ and $S^{*}_{MAX}$ show a decrement while $W^{*}_{c}$ showed a marked increase, consequently improving performance $Q^{*}$ (Fig. 6(A)–(D)). This shows that this pathway is more favourable for action selection similar to GP OT–STRD2. The model had best

performance for $w^{+}_{in-d2} = w^{-}_{ot-in} = 0$, equal to GPR model. However we used the weight of $w^{+}_{in-d2} = 0.25$ and $w^{-}_{ot-in} = -0.25$ (Fig. S2F) in the final model, which yielded best performance. Tonic level of GPi/SNr remained constant till $w^{+}_{in-d2} = 0.5$ then increased. Reversal was noticed for $w^{-}_{ot-in} = -0.25$ and $w^{+}_{in-d2} \leq 0.5$ and for DA $\geq 0.4$ indicating its role in causing reversal largely in the soft selection regime (Fig. 7(E) and Table 4), similar to GP OT–STRD2.

### 3.3. Phase 3: Combined model — I

In the third phase, combinations of connections were simulated to dissect out their function. This gave rise to a large number of simulations but essentially it was accomplished in two broad ways. We first captured the dichotomy of the GPe TI neural population — outer and inner neurons added together onto the GPR model which had a single homologous GPe , which we called *Combined model — I* and we present here two instantiations of the same as Case A and Case B.

#### 3.3.1. Combined model — I: Case A

In Case A, the GPe TI projections to striatum, $w^{+}_{ot-d1}$, $w^{+}_{ot-d2}$, $w^{+}_{in-d1}$, $w^{+}_{in-d2}$, along with GPe outer–GPe inner pathway $w^{-}_{ot-in}$, were varied (pathways 8 + 6 in Fig. 1(C)). The inhibitory same population weights were 'lesioned' $w^{-}_{ot-ot} = w^{-}_{in-in} = 0$. $H^{*}_{MAX}$ showed a marked increase while $S^{*}_{MAX}$ was reduced. $W^{*}_{c}$ shows a marked decrease. Overall, there was a decrement of performance $Q^{*}$ (Fig. 9(A)–(D)). The model showed best performance for $w^{-}_{ot-in} = -0.5$, $w^{+}_{ot-d1} = w^{+}_{ot-d2} = 0.5$ and $w^{+}_{in-d1} = w^{+}_{in-d2} = 0.25$ (Fig. S3A). Reversal was also noticed implicating the modelled pathways in causing it (see Table 4).

#### 3.3.2. Combined model — I: Case B

In Case B, the GPe TI projections to striatum were fixed $w^{+}_{ot-d1} = w^{+}_{ot-d2} = 0.5$ and $w^{+}_{in-d1} = w^{+}_{in-d2} = 0.25$. The inhibitory same population weights were varied $w^{-}_{ot-ot}$, $w^{-}_{in-in}$ along with GPe outer–GPe inner pathway $w^{-}_{ot-in}$ (pathway 4 in Fig. 1(B) + pathways 5 + 6 in Fig. 1(C)). $H^{*}_{MAX}$ showed an increase while $S^{*}_{MAX}$ showed a marked reduction. $W^{*}_{c}$ also showed a marked decrease, causing a decrement of performance $Q^{*}$ (Fig. 9(A)–(D)). The model shows best performance for $w^{-}_{ot-ot} = w^{-}_{in-in} = w^{-}_{ot-in} = -0.25$ (Fig. S3B). Reversal and changes in tonic value of GPi/SNr were noticed implicating these pathways in both of these functions (see Table 4).

### 3.4. Phase 3: Combined model — II

This second major part of combined model simulations, called *Combined model — II* augmented the combination model — I, with GPe TA neurons. We divided the model into three stages, each of which is detailed below.

#### 3.4.1. Stage 1: Inter-population connections

This model focused on varying the weights of the inter-population inhibitory weights within the GPe. The weights $w^{-}_{ot-in}$, the pathway between GPe outer and GPe inner neurons, $w^{-}_{ot-ta}$, the pathway between GPe outer and GPe TA neurons, $w^{-}_{in-ta}$, the pathway between GPe inner and GPe TA neurons were varied (pathway 3 in Fig. 1(B) + pathway 6 in Fig. 1(C)). The GPe TI projections to striatum, were set to zero, $w^{+}_{ot-d1} = w^{+}_{ot-d2} = w^{+}_{in-d1} = w^{+}_{in-d2} = 0$. $H^{*}_{MAX}$ and $S^{*}_{MAX}$ showed an increase. $W^{*}_{c}$ however, showed a marked decrease resulting in a decrement of performance $Q^{*}$ (Fig. 9(A)–(D)). Best performance of the model was for the weights $w^{-}_{ot-in} = 0$ and $w^{-}_{ot-ta} = w^{-}_{in-ta} = -1$ (Fig. S3C). The role of GP OT–GP IN pathway in reversal as well as in influencing tonic value of GPi/SNr were confirmed. It also became apparent here that using the other two pathways GP OT–GPe TA and GP IN–GPe TA, the GPe TI neurons control the activity of the TA neurons and maintain their influence over the striatum.

#### 3.4.2. Stage 2: Intra-population connections

This model added onto stage 1, the within population inhibitory pathways, which were fixed in the former. The weights in stage 1 along with $w^{-}_{ot-ot}$, $w^{-}_{in-in}$ and $w^{-}_{ta-ta}$ were varied (pathways 3 + 4 + 1 in Fig. 1(B) +pathways 6 + 5 in Fig. 1(C)). This led to a large number of simulations with many instantiations having performances greater than the GPR model. Only the projections from the GPe TI neurons to the striatum were 'lesioned', $w^{+}_{ot-d1} = w^{+}_{ot-d2} = w^{+}_{in-d1} = w^{+}_{in-d2} = 0$. $H^{*}_{MAX}$ and $S^{*}_{MAX}$ showed an increase. $W^{*}_{c}$ however showed a marked decrease resulting in a decrement of performance $Q^{*}$ (Fig. 9(A)–(D)). Best performance occurs for $w^{-}_{ot-in} = w^{-}_{ot-ot} = w^{-}_{in-in} = w^{-}_{ta-ta} = -0.25$ and $w^{-}_{ot-ta} = w^{-}_{in-ta} = -0.5$ (Fig. S3D). The intra-population connections of the GPe TI neurons were confirmed to be involved in influencing the tonic value of GPi/SNr and in reversal. However, the GPe TA–GPe TA pathway did not seem to partake in any function nor contribute to selection (see Table 4).

#### 3.4.3. Stage 3: Extended architecture

This model incorporated the extended architecture we planned to simulate (Fig. 1(D)). The set of weights for best performance selected from this model is presented as the final model.

### 3.5. Final model

The weights were $w^{-}_{ta-d1} = w^{-}_{ta-d2} = -0.75$, $w^{-}_{ot-in} = -0.3$, $w^{-}_{ot-ta} = w^{-}_{in-ta} = -0.5$ and $w^{-}_{ot-ot} = w^{-}_{in-in} = w^{-}_{ta-ta} = -0.75$. The GPe outer and GPe inner to SNr, output pathway weights were set to $w^{-}_{ot-snr} = w^{-}_{in-snr} = -0.4$. We called this model Fin 1 (Fig. S3E). We also show a variant of the final model which had a higher Max $P_h$ when there was a difference in the output weights to SNr from the GPe outer and GPe inner neurons, $w^{-}_{ot-snr} = -1$ $w^{-}_{in-snr} = -0.2$. We called this model Fin 2 (Fig. S3F).

*Fin 1.* $H^{*}_{MAX}$ showed an increase while $S^{*}_{MAX}$ showed a slight decrease. $W^{*}_{c}$ showed a slight decrease, but the overall performance $Q^{*}$ showed a slight but clear increase than the GPR model (Fig. 9(A)–(D)). Of all the combined models, this was the only model which showed an increase in performance indicating that the complete architecture was necessary to perform optimal action selection. The model also had reversal largely in the soft selection regime (Fig. 7(F)), thus reducing promiscuous selection. Thus, the model performs better selection *per se* than the GPR model, along with the added functionalities derived from the extended connectivity which are detailed below.

*Fin 2.* This model tested the differences in output weights to GPi/SNr from GPe TI neurons. Best performance occurred for $w^{-}_{ot-snr} = -0.8$ and $w^{-}_{in-snr} = -0.2$. Although $H^{*}_{MAX}$ showed an increase, $S^{*}_{MAX}$ and $W^{*}_{c}$ showed a decrement bringing down the model performance $Q^{*}$ (Fig. 9(A)–(D)). The results confirmed the stepwise model results and showed that higher weights on outer neuron projections to the output nuclei promoted easier selection, compared to the inner neuron projections to the output nuclei.

### 3.6. New control functions of GPe

In the original GPR model, routes through GPe were interpreted as 'control pathways' since GPe supplied signals to ensure that the main 'selection pathway' worked correctly (Fig. 1(A)). Some of our modelling results have an interpretation within this context, highlighting new control properties of the GPe.

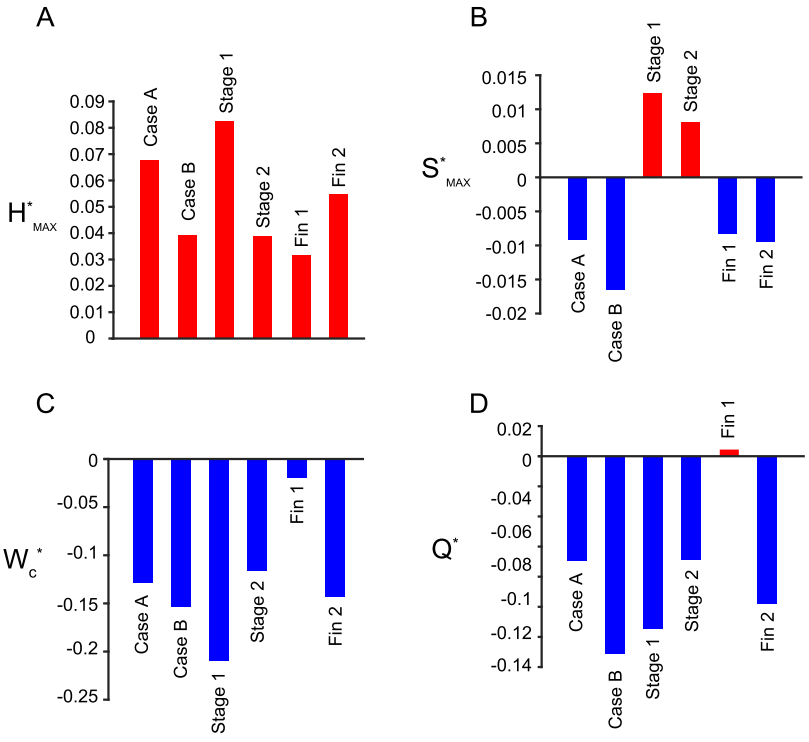


**Fig. 9.** *Performance metrics.* Performance metrics for the combined models **(A)** $H^*_{MAX}$ values showing the relative change in Hard selection of the combined models to that of the GPR model **(B)** $S^*_{MAX}$ values showing the relative change in Soft selection of the combined models to that of the GPR model **(C)** $W^*_c$ values showing the relative change in cross-over point of the combined models to that of the GPR model **(D)** $Q^*$ Performance metric values of combined models relative to the GPR model. In all, red plots indicate increment in value while blue plots indicate decrement in value. (For interpretation of the references to colour in this figure legend, the reader is referred to the web version of this article.)

### 3.6.1. The striatal switch network

The arkypallidal TA neurons can act as a 'striatal switch' and with increased activity, can essentially 'switch off' the striatum (Table 4). The prototypical outer and inner neurons maintain control over the striatum through the TA neurons and by inhibiting their activity can 'turn on' the striatum. The crucial link is the TI (outer/inner) — TA connection through which the TI neurons can operate the 'switch'. STN also plays an important role in the operation of the switch, in that by exciting the TA neurons they can 'switch off' the striatum (see also Discussion). Thus, we can dissect out the 'striatal switch network' consisting of the striatal D2–GPe TA pathway which initiates the network, the GPe TI–GPe TA and STN–GPe TA pathways which operate the switch and the GPe TA–STR pathways which execute the function of the 'switch' (See Table 4 and Fig. 10(A)). This is also the network which produces oscillations for low dopamine values, and hence could be a potential source for Parkinsonian oscillations (Fig. 5).

### 3.6.2. SNr control network

The TI (outer/inner) neurons control the GPi/SNr — the output nuclei, by setting the tonic level of inhibition the GPi/SNr have on their efferents, in turn, maintaining control over the basal ganglia output. Through the same population inhibitory pathways and the GPe OT–GPe IN pathway, the outer and inner neurons can increase the tonic activity of the output nuclei (Fig. 8(A), Table 4). Through their projections to the output nuclei, the outer and inner neurons can turn down the activity of GPi/SNr (Fig. 8(B), Table 4). This ability to influence basal ganglia output gives the GPe prototypical neurons effective control of selection. In this, the outer neurons are 'soft selectors' since they facilitate selection at lower saliences, while the inner neurons are 'hard selectors' owing to their requiring higher saliences to result in selection (Fig. 10(D)). The network of these pathways which form the 'SNr control network' are shown in Fig. 10(B).

### 3.6.3. Reversal network

Through their same population inhibitory connections, the TI (outer/inner) neurons give rise to the reversal phenomenon (Fig. 7(A) & (B), Table 4). They maintain reversal across dopamine levels through their projections to the striatum (Fig. 7(D) & (E), Table 4). The outer-inner pathway does not generate reversal, but is crucial to sustain it (Fig. 7(C), Table 4), and if 'lesioned', reversal phenomenon is lost. This is due to upsetting of the two-stage processing of outer and inner neurons (Fig. 10(D), see Discussion). The pathways comprising the 'reversal network' are shown in Fig. 10(C).

## 4. Discussion

We have investigated the newly discovered intrinsic connectivity of GPe in considerable detail. Quantitative evaluation of selection performance in this model has revealed several new functions of GPe that may be understood within the selection framework. The prototypical neurons have been shown to be the principal subpopulation influencing action selection. The arkypallidal neurons are used by both the prototypical neurons and the STN, to modulate the activity of the striatum. These arkypallidal neurons are also revealed as a novel source of theta oscillations in the absence of dopaminergic modulation in the striatum. The prototypical neurons furthermore, exert their influence on the output nuclei GPi/SNr, by setting the level of their tonic activity. We can thus infer from the results, that the GPe is a nucleus of vital importance for action selection playing a range of roles in its control and modulation.

### 4.1. Support for action selection hypothesis

The action selection hypothesis (Gurney et al., 2004) is further supported by the present results. The incorporation of more

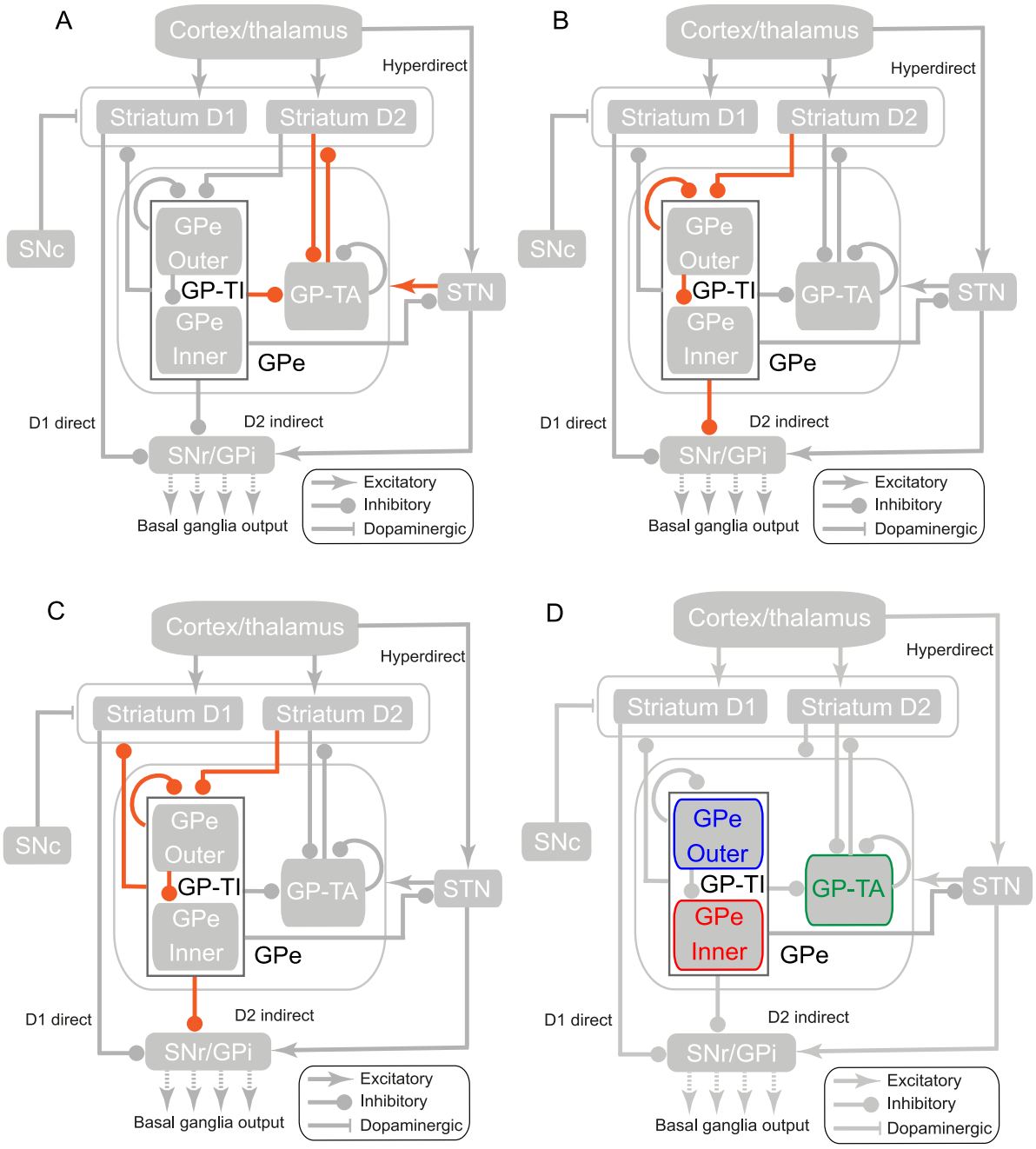


**Fig. 10.** *Functional roles of the control pathway.* Functional networks (in orange) **(A)** Striatal switch **(B)** SNr Control **(C)** Reversal **(D)** Population functions — the GPe inner neurons (red) are *hard selectors*, the GPe outer neurons (blue) are *soft selectors* and the GPe TA neurons (green) are the *striatal switch*. (For interpretation of the references to colour in this figure legend, the reader is referred to the web version of this article.)

anatomically plausible detail (compared with the original, GPR model), and the optimisation of the model on action selection capabilities show quantitative improvement in selection. Moreover, new functional roles of the control pathway have emerged along with a greater understanding of the roles of neural subpopulations within the GPe. Earlier models with the classical connectivity of the basal ganglia did demonstrate the ability to perform action selection. However, this had not been addressed with the newly revealed projections and connectivity of the GPe.

### 4.2. TA neurons can turn up or turn down striatal activity

Our results indicate that the arkypallidal TA neurons, through their activity, can turn down activity in the striatum and can be regarded as a sort of striatal 'switch' (Fig. 10(D)). Furthermore, the prototypical TI neurons through their modulation of the TA neuronal excitability, can restore striatal activity. The GPe TI–GPe TA pathway seems to be the crucial link through which the TI neurons control the TA neurons, in turn maintaining operational control over the striatum. There is some evidence from modelling indicating a strong GPe TI–TA projection (Lindahl & Hellgren Kotaleski, 2016). In our simulations, for high weights on the arkypallidal projections to striatum, activity in striatum was very low, and the TA neurons had effectively turned striatum 'off'. This resulted in no selection occurring. As soon as the weights on the arkypallidal projections to striatum were reduced, activity in the striatum was restored and selection was induced, with performance metric $Q^*$ higher than the GPR model. The striatum had been turned 'on'.

**Table 4**
Functions of different pathways.

| Pathway | Oscillations | Striatal Switch | Reversal | Tonic level of GPi/SNr | Network |
|---|---|---|---|---|---|
| GPe TA to striatum D1 | Generates | Executes | – | – | Striatal switch |
| GPe TA to striatum D2 | Generates | Executes | – | – | Striatal switch |
| GPe TA to GPe TA | – | – | – | – | – |
| GPe TI (outer/inner) to GPe TA | – | Operates | – | – | Striatal switch |
| STN to GPe TA | – | Operates | – | – | Striatal switch |
| GPe outer to GPe outer | – | – | Generates | Increases | Reversal/GPi/SNr control |
| GPe inner to GPe inner | – | – | Generates | Increases | Reversal/GPi/SNr control |
| GPe outer to GPe inner | – | – | Sustains | Increases | Reversal/GPi/SNr control |
| GPe outer to GPi/SNr | – | – | Executes | Decreases | Reversal/GPi/SNr control |
| GPe inner to GPi/SNr | – | – | Executes | Decreases | Reversal/GPi/SNr control |
| GPe outer to striatum D1 | – | – | In the hard selection regime | – | Reversal |
| GPe outer to striatum D2 | – | – | In the soft selection regime | – | Reversal |
| GPe inner to striatum D1 | – | – | In the hard selection regime and intermediate DA | – | Reversal |
| GPe inner to striatum D2 | – | – | In the soft selection regime | – | Reversal |
| Striatum D2 to GPe TI (outer/inner) | – | – | Initiates | Initiates | Reversal/GPi/SNr control |
| Striatum D2 to GPe TA | Initiates | Initiates | – | – | Striatal switch |
| Striatum D1 to GPi/SNr | – | – | – | – | Direct pathway |
| STN to GPe TI (outer/inner) | – | Operates | – | – | Striatal switch |
| STN to GPi/SNr | – | – | – | – | Hyperdirect pathway |

Functions of the different pathways simulated in our models and the network architecture that they belong to. The GPe TA projections give rise to oscillations but input from the striatum D2 to the GPe TA initiates them. The 'Striatal switch' function is executed via the GPe TA projections to the striatal SPNs. The 'switch' is operated by both the STN and GPe TI(outer/inner). 'Reversal' is generated by the same subpopulation inhibitory connections of the GPe TI (outer/inner) neurons, while the outer-inner projection is needed to maintain it. The striatal projections of the outer/inner neurons ensure that reversal occurs across the range of dopamine activity in the striatum, while reversal eventually occurs via the GPe TI projections to the output nuclei GPi/SNr.

These results are supported by a recent study which showed that arkypallidal TA neurons in the GPe, send a 'Stop' signal and can essentially curtail developing action representations in the striatum (Mallet et al., 2016). Although it is not clear whether the arkypallidal cells are the source or simply relay this 'Stop' signal as noted in Mallet et al. (2016), our simulations suggest that the GPe TI prototypical cells could have a role in determining when the arkypallidal cells can 'turn off' the striatum.

Another factor to consider here is the role of the STN, which is known to generate a stop signal via the hyperdirect pathway (Frank, 2006; Gillies & Willshaw, 1998) and the indirect pathway. STN and GPe TA neurons fire in phase with cortical activity (Mallet et al., 2012) and there is also computational evidence indicating that STN might target GPe TA neurons more strongly than GPe TI (Nevado-Holgado, Mallet, Magill, & Bogacz, 2014). Thus, the STN could clearly activate the GPe TA neurons, thereby switching-off the striatum. However, the GPe TI neurons can inhibit the GPe TA as well as the STN, thereby stopping the 'stop' signal from the STN–GPe TA network, given that the GPe TI neurons fire out of phase with cortical activity (Mallet et al., 2012). Thus, both the STN and the GPe TI contribute to the striatal switch network, and they *operate* the switch — in that STN can turn the switch 'on', while the GPe TI can turn it 'off'. This also suggests the possibility of both the STN and the prototypical GPe neurons being involved in *explorative* behaviour. Along with the tonic dopaminergic modulation of the striatum, there have been suggestions of the involvement of the STN–GPe network, as well as the lateral intrinsic connectivity within the STN in explorative behaviour (Chakravarthy, Joseph, & Bapi, 2010; Gillies, Willshaw, & Li, 2002; Kalva, Rengaswamy, Chakravarthy, & Gupte, 2012; Mandali, Rengaswamy, Chakravarthy, & Moustafa, 2015). More work is required with our model to explore these possibilities, but the model provides a basis for doing so in future simulations.

### *4.3. Oscillations from TA neuronal projections — consistent with Parkinsons disease*

Modelling of the arkypallidal TA neurons has revealed low-frequency theta oscillations (3–10 Hz) which are reliant on the GPe TA — striatal pathway. Low frequency oscillations have been associated with Parkinsons disease and are said to be in synchrony with tremor (Bevan, Magill, Terman, Bolam, & Wilson, 2002). Oscillations around this range are said to arise in the basal ganglia and spread to the cortex, producing an 'antikinetic' effect (Hutchison et al., 2004). Loss of dopamine has been associated to these oscillations (Rivlin-Etzion et al., 2006; Weinberger & Dostrovsky, 2011). Furthermore, modelling also suggests that increase in oscillations interfering with information processing in the basal ganglia is characteristic of Parkinsonian conditions (Bergman et al., 1998; Lindahl & Hellgren Kotaleski, 2016). Our model shows that the oscillations have maximum amplitude for no dopamine activity (DA = 0) consistent with Parkinsons disease, and are suppressed for higher dopamine values. The model reveals TA projections to the striatum to be the source of these low frequency oscillations, but high inhibitory input from the prototypical TI neurons are also necessary to sustain them. The model also shows better performance for a corresponding high inhibitory weight of TI (outer/inner) — TA pathways, which are accordingly set high in the final model. Furthermore, the GPe TI neurons are known to have more axonal collaterals within GPe, targeting GPe TA neurons (Lindahl & Hellgren Kotaleski, 2016; Sadek et al., 2007). There is also evidence implicating the GPe TA neurons as well as the GPe–STN network in inducing oscillations (Lindahl & Hellgren Kotaleski, 2016; Nevado-Holgado et al., 2014). In summary, we can conclude from our results that the anatomical substrate exists to sustain these oscillations, and without dopamine, there may be no stopping them.

While beta oscillations are discussed more often in relation to Parkinson's disease, theta oscillations are associated with a very

characteristic pathological deficit — freezing of gait. Clinical studies show an increase of theta oscillations with freezing, referred to as 'trembling in place' (Plamen, Olivier, & Thomas, 2006; Shine et al., 2014). It has been hypothesised that oscillatory interaction in the STN–GPe network underly these oscillations (Shine et al., 2013). Our results show that the oscillations manifest when there is competition between two action representations (See Fig. 5).

It thus appears that the arkypallidal TA neurons are a novel potential source of theta oscillations under dopamine depleted conditions, similar to pathophysiological conditions of Parkinsons disease. But how are they generated? Our results clearly reveal the cause — lack of dopamine. Dopamine is well known to modulate excitability of the SPNs in the striatum (Harsing & Zigmond, 1997; Humphries, Lepora et al., 2009) and our results show that the arkypallidal neurons are able to turn up or turn down the activity of the SPNs via their massive projections. Our results indicate that removing dopamine could alter the excitability of SPNs during high salience competing inputs, resulting in a continuous switching between the 'striatum on' and 'striatum off' conditions (translates to switching between their 'up' and 'down' states (Kasanetz, Riquelme, O'Donnell, & Murer, 2006; Wilson & Groves, 1981)), which would also engage the STN–GPe, inducing the theta oscillations in the network. This possibility is corroborated by the suggestion that rhythmic inputs from striatum, but also from cortex and thalamus could engage STN-globus pallidus network in Parkinsonian oscillations (Nevado-Holgado et al., 2014). Furthermore, these oscillations seen in the STN–GPe–GPi/SNr network (see Fig. 5(E) & (F)) agree with the evidence of high level of synchronous oscillations, including the theta band, observed in these nuclei in Parkinsonian conditions (Tachibana, Iwamuro, Kita, Takada, & Nambu, 2011; Weinberger & Dostrovsky, 2011).

Our model also suggests a possible explanation for a long standing paradox in PD treatment. Current treatment therapies to alleviate parkinsonian deficits by lesions and deep-brain stimulations of the STN present an incongruity — in that both lesioning of the STN, or its increased activity (by high frequency deep brain stimulation) reduces Parkinsonian symptoms (Benabid, Chabardes, Mitrofanis, & Pollak, 2009; Okun & Vitek, 2004). Our results also indicated that mimicking these conditions in the model which produced the oscillations under dopamine depleted conditions could remove the oscillations and improve selection (See Results and Figs. 5(G), (H) and S4). Our network architecture for the striatal-switch (Fig. 10(A)) suggests that lesioning STN, would result in the lesser activation of the GPe TA, preventing the inhibition of SPNs, which means that the striatal switch architecture would simply be bypassed — thus preventing oscillations in the network. This hypothesis is supported by several of our step-wise models, which lacked the GPe TA neurons, for instance, the GPe TI–GPe TI step-wise model. Although the striatal switch network was absent, the model could perform action selection *per se*, as well as the GPR model (Fig. 6(A)–(D)).

On the other hand, high-frequency stimulation of the STN would 'switch-on' the GPe TA — but this would also activate the GPe TI neurons, which would play their part in controlling STN excitation as well as in inhibition and 'switch-off, of the GPe TA neurons. We speculate that this activation of the GPe TA from STN and the consequent modulation of their excitability by the TI neurons, would inhibit the SPNs in striatum to prevent their oscillatory swapping between 'on' and 'off' states caused by lack of dopamine.

Lastly, with respect to the preferential targets of the massive arkypallidal projections to striatum, there is by far, no clear consensus. However, there is evidence suggesting that they target not only the spines of the SPNs, but also different interneuron subtypes (Burke et al., 2017; Glajch et al., 2016; Hegeman et al., 2016; Mallet et al., 2012). We have modelled only the diffuse arkypallidal inhibitory projections to the SPNs. The final model gave best performance for a lower weight of the arkypallidal projections to SPNs (see Results), which corroborates anatomical evidence indicating that the projections are not exclusive to the striatal SPNs.

### 4.4. GPe TA predominantly receive local collaterals from GPe TI neurons

Our results indicated that the probability of GPe TI–GPe TA connections were more likely, rather than GPe TA–GPe TA connections. While in the step-wise models, both the pathways showed similar performance (see Fig. 6(A)–(D)), subsequent combined models revealed no role for the GPe TA–GPe TA pathway. Furthermore, change of weights of the TA–TA did not result in any change in performance. However, the GPe TI–GPe TA pathway was a vital component of the striatal switch network, enabling the TI neurons to control the TA neurons. While it is generally known that GPe neurons receive local collaterals, the organisation of local collateral inputs to the GPe TA neurons is not yet clear. However, it is known that the TI neurons send out more local collaterals than the TA neurons (Mallet et al., 2012), and that they are also the predominant subpopulation, indicating a stronger TI–TA connection probability. This allows us to predict that a TI–TA pathway is more likely, which also agree with those of Lindahl and Hellgren Kotaleski (2016), which predict a stronger TI–TA connection.

### 4.5. Prototypical TI neurons promote better hard selection through reversal

Reversal phenomenon noticed in these simulations was another significant result. The GPR model had shown only a monotonic decrease in channel output with increase in salience or input. With the inclusion of the reversal network (Fig. 10(C)), which are essentially the prototypical neurons (see subsequent section), this trend can be reversed.

Reversal can occur as several cases, some of which can be detrimental to a selection mechanism. For instance, in the case which resulted in the deselection of a selected channel (Single Ch selection → No Selection). However, these cases were only seen in step-wise models and were not observed in the final model, indicating that they were due to an incomplete modelled architecture. In the final model, reversal cases comprised entirely of Dual channel selection → Interference/Distortion/Switching occurring in both the hard and soft selection regimes, although largely in the soft selection regime (Fig. 7(F)). This contributed to the better performance of the model than the GPR model, in that some of the soft selection outcomes were reversed into hard selection outcomes. This also indicated that the prototypical neurons aid in better *decision-making* by making a 'choice' between competing channels of high salience. Thus, when faced between two possible action outcomes, the prototypical neurons can essentially 'choose' one at a time.

The simulations have shown that within population inhibitory connections of outer and inner neurons, are responsible for causing the reversal phenomenon (Fig. 7 and Table 4). It is also evident that with higher weights they ensure reversal occurring across the range of dopamine values. High weights are also necessary for reversal to occur in subsequent combined models, in addition to their contribution for better performance. It is with this view that higher weights were fixed for these pathways in combined models, which in addition, agrees with anatomical evidence showing prototypical neurons having more extensive local collaterals (Sadek et al., 2007). In addition to the within inhibitory projections of the outer and inner neurons, the outer to inner neuron inhibitory projections are also vital for reversal, as well as for improving the performance of the model. These three pathways form the core aspect of the reversal network (Fig. 10(C)).

### 4.6. Striatal projections of prototypical TI neurons facilitate reversal over a range of dopamine levels

The striatal projections of outer and inner neurons seem to play the crucial role of spreading the reversal phenomenon across dopamine levels (Fig. 7 and Table 4). The projections of outer neurons to the selection pathway (STRD1) cause reversal at low dopamine levels DA $\leq$ 0.3, The outer neuron projections to the control pathway (STRD2) cause reversal for DA $\geq$ 0.3 onwards. Striatal projections of inner neurons to both the selection and control pathways, cause reversal for mid-valued dopamine (0.2 $\leq$ DA $\leq$ 0.8). This allows for 'reversal' of promiscuous selections into hard selection outcomes occurring at different levels of dopamine activity — aiding in more optimal selection.

Regarding the striatal projections of the prototypical neurons, from (Sadek et al., 2007), we have data indicating every 4/8 outer neurons and 2/9 inner neurons projecting to the striatum. The final model yielded best performance for matching corresponding weights at 0.5 and 0.25 respectively. Having higher weights on outer neuron striatal projections resulted in complete soft selection, while higher weights on inner neuron striatal projections resulted in no selection occurring. Thus, the best performance weights in the final model shows a degree of agreement on available biological data on these pathways.

### 4.7. Differences in prototypical TI neural population influences

The outer neurons seem to be associated more with soft selection owing to the decreased tonic level of the GPi/SNr they set, through their efferents. This allows action representations with relatively lower saliences to be selected. This was further substantiated in the final model, wherein an increased weight of outer-SNr pathway and decreased weight of inner-SNr pathway increased the hard selection performance $H^*_{MAX}$ (Fin 2, see Results). Although $H^*_{MAX}$ was increased, there was a decrease of $W^*_c$ and the performance was less than the GPR model. The range of dopamine values where hard selection dominates was reduced considerably (Fig. S3F) because this condition allows for more promiscuous selection, which decreases performance. Overall, this indicates that the outer neurons can help in easier selection making them 'soft selectors' (Fig. 10(D)).

In contrast, the inner neurons seem to be more associated with hard selection (Fig. 10(D)), since they reduce the tonic level of GPi/SNr to a much less extent than the outer neurons. Thus, the inner neurons encourage only actions with stronger saliences to be selected thus reducing promiscuous selection — making them 'hard selectors'. Additionally, we verified this by running a variant of the Fin 2 model with higher inner neuron to GPi/SNr and reduced outer to GPi/SNr weights. The extent of hard selection regime across dopamine values did increase. However, maximum value of hard selection was less than that of the Fin 1 model which had the outer and inner neuron to GPi/SNr weights equal.

The overall conclusion was that both the differential influences of the outer and inner neurons, on soft and hard selection are necessary to promote optimal selection. In the final model, the best performance was for having equal weights on these two pathways. This allows us to predict that the outer and inner neuron efferents to the GPi/SNr are relatively equal in magnitude and strength. There is no evidence so far to support any differences in the relative strengths of the extrinsic efferents of outer and inner neurons to the GPi/SNr, as of yet.

### 4.8. GPe influence on the GPi/SNr

The within population inhibitory pathways of the outer and inner neurons and the outer–inner pathway, increase the tonic value of GPi/SNr with increasing weights which results in higher salience being required to reach the selection threshold (Fig. 8(A)). The extrinsic efferents of the GPe outer and inner neurons to GPi/SNr, tend to decrease the tonic value of GPi/SNr, making it easier to reach the threshold (Fig. 8(B)). Since the weight change in the semilinear neuron is equivalent to changing afferent drive, this indicates a 'push–pull' mechanism, wherein, based on the relative 'importance' of a particular action, the feasibility of its selection can be enhanced or decreased by the prototypical neurons. This reveals an additional mechanism, through which the GPe can maintain an operational control over the GPi/SNr; without the GPe prototypical neurons, there would be no modulation of the level of tonic activity of the GPi/SNr. Lesion studies of the GPe result in a marked increase in the level of tonic activity of the GPi/SNr, as well as exacerbated Parkinsonian symptoms (Zhang, Russo, Mewes, Rye, & Vitek, 2006). Our results agree in that lesions of the outer-SNr and inner-SNr pathways leads to the loss of the 'push' mechanism, and hence induces difficulty in selection. The outer-SNr pathway lesion reduces the ability for soft selection, while the inner-SNr pathway lesion results in reduced ability for hard selection. Lesions of outer-outer and inner–inner pathways result in loss of the 'pull' mechanism — as well as loss of reversal.

## 5. Concluding remarks

The simulations have thrown light on the importance of the GPe in the basal ganglia, and its crucial and myriad role in action selection. It seems to be a 'control centre' of the basal ganglia with considerable influence on the functioning of other basal ganglia nuclei. The results show the GPe controlling the striatum, the GPi/SNr and as shown also in previous models, the STN (Gurney et al., 2001a). In particular, the prototypical GPe TI (outer/inner) neurons, seem to be the 'controllers', maintaining operational control over different subnuclei, and on striatum via the arkypallidal TA neurons. They can use the arkypallidal neurons to turn on or turn off the striatum, can effect selection by setting the level of tonic activity of the GPi/SNr, and can contribute to optimising action selection via reversal.

The implication is that the GPe cannot be modelled as a simple uniform relay nucleus. On the contrary, each subpopulation plays a distinct and direct role in action selection. The arkypallidal neurons clearly have a massive influence on the striatum and when more data is available on their connectivity, they must be incorporated in future models. Our model has allowed for the unification of the two levels of neuronal organisation in the GPe — the prototypical neurons and the outer/inner neurons. These subtypes of the prototypical neurons also have differences in their influence on action selection. The prototypical neurons along with the tonic dopaminergic activity from the SNc in striatum, may also play a role in explorative behaviours. Furthermore, their ability to regulate the tonic level of activity of the output nuclei (GPi/SNr) in a 'push–pull' manner could also indicate a role in learning. Thus, the indirect pathway would seem to have a wider scope of functionality in addition to being the classical 'no-go' pathway. Overall, the simulations have reinforced the hypothesis of action selection as a primary function of the basal ganglia.

Looking forward, the simulation results open up new questions. For instance, the ability of the arkypallidal neurons to suppress action representations and the ability of the STN–GPe prototypical network to 'use' this function, leads to the question whether these decisions are made at the level of the basal ganglia? Does the GPe, and more specifically the prototypical neurons themselves, have a

part in the decision-making? Or are they merely relaying inputs? The range of roles the GPe has in action selection as suggested by our simulation results, hint at a more proactive role in decision-making rather than being just a relay of decisions made elsewhere. Although we have modelled to a considerable extent, the intrinsic connectivity of the GPe known till date, we are yet to capture the connectivity *in toto*. The extended architecture proposed however, must be simulated in the much wider contexts of cortical and thalamic loops as well as the intrinsic and extrinsic connectivity of other basal ganglia nuclei.

Finally, the involvement of the GPe–STN–GPi/SNr network in generating oscillations and in particular, the arkypallidal projections to striatum, demand for more comprehensive circuit investigations in pathological conditions of the basal ganglia like Parkinson's disease. These results can act as useful pointers for clinical assessment as well as remedy for these pathological conditions. However, as with all our results, we look forward to their being extended and tested further against new data.

## Acknowledgements

We acknowledge the following grant sponsors: European Horizon 2020 Framework Programme (Grant 720270 (Human Brain Project SGA1), Grant 785907 (Human Brain Project SGA2)), the Swedish Research Council and the Swedish e-Science Research Center. We are also grateful for comments on the manuscript by Dr. Brita Robertson and Associate professor Dr. Peter Wallén.

## Appendix A. Supplementary data

Supplementary material related to this article can be found online at https://doi.org/10.1016/j.neunet.2018.10.003.

## References

Abdi, A., Mallet, N., Mohamed, F. Y., Sharott, A., Dodson, P. D., Nakamura, K. C., … , & Magill, P. J. (2015). Prototypic and arkypallidal neurons in the dopamine-intact external globus pallidus. *Journal of Neuroscience*, *35*(17), 6667–6688.

Akkal, D., Burbaud, P., Audin, J., & Bioulac, B. (1996). Responses of substantia nigra pars reticulata neurons to intrastriatal D1 and D2 dopaminergic agonist injections in the rat. *Neuroscience Letters*, *213*(1), 66–70.

Alexander, G. E., DeLong, M. R., & Strick, P. L. (1986). Parallel organization of functionally segregated circuits linking basal ganglia and cortex. *Annual Review of Neuroscience*, *9*(1), 357–381. PMID: 3085570.

Bahuguna, J., Tetzlaff, T., Kumar, A., Hellgren Kotaleski, J., & Morrison, A. (2017). Homologous basal ganglia network models in physiological and Parkinsonian conditions. *Frontiers in Computational Neuroscience*, *11*, 79.

Barto, A. G. (1994). Reinforcement learning control. *Current Opinion in Neurobiology*, *4*(6), 888–893. URL http://www.sciencedirect.com/science/article/pii/0959438894901384.

Barto, A. G., & Mahadevan, S. (2003). Recent advances in hierarchical reinforcement learning. *Discrete Event Dynamic Systems*, *13*(4), 341–379. https://doi.org/10.1023/A:1025696116075.

Beiser, D. G., & Houk, J. C. (1998). Model of cortical-basal ganglionic processing: Encoding the serial order of sensory events. *Journal of Neurophysiology*, *79*(6), 3168–3188.

Benabid, A. L., Chabardes, S., Mitrofanis, J., & Pollak, P. (2009). Deep brain stimulation of the subthalamic nucleus for the treatment of Parkinson's disease. *The Lancet Neurology*, *8*(1), 67–81. URL http://www.sciencedirect.com/science/article/pii/S1474442208702916.

Bergman, H., Feingold, A., Nini, A., Raz, A., Slovin, H., Abeles, M., et al. (1998). Physiological aspects of information processing in the basal ganglia of normal and Parkinsonian primates. *Trends in Neurosciences*, *21*(1), 32–38. URL http://www.sciencedirect.com/science/article/pii/S016622369701151X.

Berthet, P., Lindahl, M., Tully, P. J., Hellgren-Kotaleski, J., & Lansner, A. (2016). Functional relevance of different basal ganglia pathways investigated in a spiking model with reward dependent plasticity. *Frontiers in Neural Circuits*, *10*, 53.

Bevan, M. D., Booth, P. A. C., Eaton, S. A., & Bolam, J. P. (1998). Selective innervation of neostriatal interneurons by a subclass of neuron in the globus pallidus of the rat. *Journal of Neuroscience*, *18*(22), 9438–9452.

Bevan, M. D., Magill, P. J., Terman, D., Bolam, J., & Wilson, C. J. (2002). Move to the rhythm: oscillations in the subthalamic nucleus–external globus pallidus network. *Trends in Neurosciences*, *25*(10), 525–531.

Blenkinsop, A., Anderson, S., & Gurney, K. (2017). Frequency and function in the basal ganglia: the origins of beta and gamma band activity. *The Journal of Physiology*, *595*(13), 4525–4548.

Bogacz, R., Martin Moraud, E., Abdi, A., Magill, P. J., & Baufreton, J. (2016). Properties of neurons in external globus pallidus can support optimal action selection. *PLoS Computational Biology*, *12*(7), 1–28. https://doi.org/10.1371/journal.pcbi.1005004.

Bolam, J. P., Hanley, J. J., Booth, P. A. C., & Bevan, M. D. (2000). Synaptic organisation of the basal ganglia. *Journal of Anatomy*, *196*(4), 527–542. http://dx.doi.org/10.1046/j.1469-7580.2000.19640527.x.

Brown, J. W., Bullock, D., & Grossberg, S. (2004). How laminar frontal cortex and basal ganglia circuits interact to control planned and reactive saccades. *Neural Networks*, *17*(4), 471–510.

Burke, D. A., Rotstein, H. G., & Alvarez, V. A. (2017). Striatal local circuitry: A new framework for lateral inhibition. *Neuron*, *96*(2), 267–284. http://dx.doi.org/10.1016/j.neuron.2017.09.019.

Calabresi, P., Picconi, B., Tozzi, A., Ghiglieri, V., & Di Filippo, M. (2014). Direct and indirect pathways of basal ganglia: a critical reappraisal. *Nat Neurosci*, *17*(8), 1022–1030. http://dx.doi.org/10.1038/nn.3743.

Chakravarthy, V. S., & Balasubramani, P. P. (2013). Basal ganglia system as an engine for exploration. In D. Jaeger, & R. Jung (Eds.), *Encyclopedia of computational neuroscience* (pp. 1–15). New York, NY: Springer New York.

Chakravarthy, V. S., Joseph, D., & Bapi, R. S. (2010). What do the basal ganglia do? A modeling perspective. *Biological Cybernetics*, *103*(3), 237–253. https://doi.org/10.1007/s00422-010-0401-y.

Chang, H., Wilson, C., & Kitai, S. (1981). Single neostriatal efferent axons in the globus pallidus: a light and electron microscopic study. *Science*, *213*(4510), 915–918.

Chersi, F., Mirolli, M., Pezzulo, G., & Baldassarre, G. (2013). A spiking neuron model of the cortico-basal ganglia circuits for goal-directed and habitual action learning. *Neural Networks*, *41*(Supplement C), 212–224. Special issue on autonomous learning.

Corbit, V. L., Whalen, T. C., Zitelli, K. T., Crilly, S. Y., Rubin, J. E., & Gittis, A. H. (2016). Pallidostriatal projections promote beta oscillations in a dopamine-depleted biophysical network model. *Journal of Neuroscience*, *36*(20), 5556–5571.

Damodaran, S., Cressman, J. R., Jedrzejewski-Szmek, Z., & Blackwell, K. T. (2015). Desynchronization of fast-spiking interneurons reduces beta band oscillations and imbalance in firing in the dopamine-depleted striatum. *Journal of Neuroscience*, *35*(3), 1149–1159.

Dodson, P. D., Larvin, J. T., Duffell, J. M., Garas, F. N., Doig, N. M., Kessaris, N., … , & Magill, P. J. (2015). Distinct developmental origins manifest in the specialized encoding of movement by adult neurons of the external globus pallidus. *Neuron*, *86*(2), 501–513.

Frank, M. J. (2005). Dynamic dopamine modulation in the basal ganglia: A neurocomputational account of cognitive deficits in medicated and nonmedicated Parkinsonism. *Journal of Cognitive Neuroscience*, *17*(1), 51–72.

Frank, M. J. (2006). Hold your horses: A dynamic computational role for the subthalamic nucleus in decision making. *Neural Networks*, *19*(8), 1120–1136. Neurobiology of decision making.

Frank, M. J., Seeberger, L. C., & O'Reilly, R. C. (2004). By carrot or by stick: Cognitive reinforcement learning in Parkinsonism. *Science*, *306*(5703), 1940–1943.

Freeze, B. S., Kravitz, A. V., Hammack, N., Berke, J. D., & Kreitzer, A. C. (2013). Control of basal ganglia output by direct and indirect pathway projection neurons. *Journal of Neuroscience*, *33*(47), 18531–18539.

Gillies, A. J., & Willshaw, D. J. (1998). A massively connected subthalamic nucleus leads to the generation of widespread pulses. *Proceedings of the Royal Society of London B: Biological Sciences*, *265*(1410), 2101–2109. URL http://rspb.royalsocietypublishing.org/content/265/1410/2101.

Gillies, , Willshaw, D., & Li, Z. (2002). Subthalamic–pallidal interactions are critical in determining normal and abnormal functioning of the basal ganglia. *Proceedings of the Royal Society of London, Series B*, *269*(1491), 545. URL http://rspb.royalsocietypublishing.org/content/269/1491/545.abstract.

Glajch, K. E., Kelver, D. A., Hegeman, D. J., Cui, Q., Xenias, H. S., Augustine, E. C., … , & Chan, C. S. (2016). Npas1+ pallidal neurons target striatal projection neurons. *Journal of Neuroscience*, *36*(20), 5472–5488. URL http://www.jneurosci.org/content/36/20/5472.

Grace, A. A., Floresco, S. B., Goto, Y., & Lodge, D. J. (2007). Regulation of firing of dopaminergic neurons and control of goal-directed behaviors. *Trends in Neurosciences*, *30*(5), 220–227. Fifty years of dopamine research.

Grillner, S. (2003). The motor infrastructure: from ion channels to neuronal networks. *Nature Reviews Neuroscience*, *4*, 573 EP. http://dx.doi.org/10.1038/nrn1137.

Grillner, S., Ekeberg, Ö., Manira, A. E., Lansner, A., Parker, D., Tegnér, J., et al. (1998). Intrinsic function of a neuronal network — a vertebrate central pattern generator. Published on the World Wide Web on 8 April 1998.1. *Brain Research Reviews*, *26*(2), 184–197. URL http://www.sciencedirect.com/science/article/pii/S0165017398000022.

Grillner, S., Hellgren, J., Ménard, A., Saitoh, K., & Wikström, M. A. (2005). Mechanisms for selection of basic motor programs — roles for the striatum and pallidum. *Trends in Neurosciences*, *28*(7), 364–370. URL http://www.sciencedirect.com/science/article/pii/S0166223605001293.

Grillner, S., & Robertson, B. (2016). The basal ganglia over 500 million years. *Current Biology*, *26*(20), R1088–R1100.

Gurney, K. N., Humphries, M. D., & Redgrave, P. (2015). A new framework for cortico-striatal plasticity: Behavioural theory meets in vitro data at the reinforcement-action interface. *PLoS Biology*, *13*(1), 1–25.

Gurney , Humphries, M., Wood, R., Prescott, T. J., & Redgrave, P. (2004). Testing computational hypotheses of brain systems function: a case study with the basal ganglia. *Network. Computation in Neural Systems*, *15*(4), 263–290.

Gurney , Prescott, T., & Redgrave, P. (1998). The basal ganglia viewed as an action selection device. In L. Niklasson, M. Bodén, & T. Ziemke (Eds.), *ICANN 98: Proceedings of the 8th international conference on artificial neural networks* (pp. 1033–1038). London: Springer London.

Gurney , Prescott, T. J., & Redgrave, P. (2001a). A computational model of action selection in the basal ganglia. I. A new functional anatomy. *Biological Cybernetics*, *84*(6), 401–410.

Gurney , Prescott, T. J., & Redgrave, P. (2001b). A computational model of action selection in the basal ganglia. II. Analysis and simulation of behaviour. *Biological Cybernetics*, *84*(6), 411–423.

Harsing, L. H., Jr., & Zigmond, M. (1997). Influence of dopamine on GABA release in striatum: evidence for D1–D2 interactions and non-synaptic influences. *Neuroscience*, *77*(2), 419–429.

Hegeman, D. J., Hong, E. S., Hernández, V. M., & Chan, C. S. (2016). The external globus pallidus: progress and perspectives. *European Journal of Neuroscience*, *43*(10), 1239–1265.

Hernández, V. M., Hegeman, D. J., Cui, Q., Kelver, D. A., Fiske, M. P., Glajch, K. E., … , & Chan, C. S. (2015). Parvalbumin + neurons and Npas1 + neurons are distinct neuron classes in the mouse external globus pallidus. *The Journal of Neuroscience*, *35*(34), 11830.

Hikosaka, O., Takikawa, Y., & Kawagoe, R. (2000). Role of the basal ganglia in the control of purposive saccadic eye movements. *Physiological Reviews*, *80*(3), 953–978.

Humphries, M., & Gurney, K. (2002). The role of intra-thalamic and thalamocortical circuits in action selection. *Network. Computation in Neural Systems*, *13*(1), 131–156. PMID: 11873842.

Humphries, M., Khamassi, M., & Gurney, K. (2012). Dopaminergic control of the exploration–exploitation trade-off via the basal ganglia. *Frontiers in Neuroscience*, *6*, 9. URL https://www.frontiersin.org/article/10.3389/fnins.2012.00009.

Humphries, M., Lepora, N., Wood, R., & Gurney, K. (2009). Capturing dopaminergic modulation and bimodal membrane behaviour of striatal medium spiny neurons in accurate, reduced models. *Frontiers in Computational Neuroscience*, *3*, 26.

Humphries, M. D., Stewart, R. D., & Gurney, K. N. (2006). A physiologically plausible model of action selection and oscillatory activity in the basal ganglia. *Journal of Neuroscience*, *26*(50), 12921–12942.

Humphries, M. D., Wood, R., & Gurney, K. (2009). Dopamine-modulated dynamic cell assemblies generated by the {GABAergic} striatal microcircuit. *Neural Networks*, *22*(8), 1174–1188. Cortical microcircuits.

Hutchison, W. D., Dostrovsky, J. O., Walters, J. R., Courtemanche, R., Boraud, T., Goldberg, J., et al. (2004). Neuronal oscillations in the basal ganglia and movement disorders: Evidence from whole animal and human recordings. *Journal of Neuroscience*, *24*(42), 9240–9243.

Kalva, S. K., Rengaswamy, M., Chakravarthy, V. S., & Gupte, N. (2012). On the neural substrates for exploratory dynamics in basal ganglia: A model. *Neural Networks*, *32*, 65–73. URL http://www.sciencedirect.com/science/article/pii/S0893608012000603.

Kamali Sarvestani, I., Lindahl, M., Hellgren Kotaleski, J., & Ekeberg, Ö. (2011). The arbitration-extension hypothesis: a hierarchical interpretation of the functional organization of the basal ganglia. *Frontiers in Systems Neuroscience*, *5*, 13.

Kasanetz, F., Riquelme, L. A., O'Donnell, P., & Murer, M. G. (2006). Turning off cortical ensembles stops striatal up states and elicits phase perturbations in cortical and striatal slow oscillations in rat in vivo. *The Journal of Physiology*, *577*(1), 97–113. http://dx.doi.org/10.1113/jphysiol.2006.113050.

Kim, H. F., & Hikosaka, O. (2015). Parallel basal ganglia circuits for voluntary and automatic behaviour to reach rewards. *Brain*, *138*(7), 1776–1800. http://dx.doi.org/10.1093/brain/awv134.

Kravitz, A. V., Freeze, B. S., Parker, P. R. L., Kay, K., Thwin, M. T., Deisseroth, K., et al. (2010). Regulation of Parkinsonian motor behaviours by optogenetic control of basal ganglia circuitry. *Nature*, *466*(7306), 622–626.

Lindahl, M., & Hellgren Kotaleski, J. (2016). Untangling basal ganglia network dynamics and function: Role of dopamine depletion and inhibition investigated in a spiking network model. *eNeuro*, *3*(6).

Lindahl, M., Kamali Sarvestani, I., Ekeberg, Ö., & Kotaleski, J. (2013). Signal enhancement in the output stage of the basal ganglia by synaptic short-term plasticity in the direct, indirect, and hyperdirect pathways. *Frontiers in Computational Neuroscience*, *7*, 76.

Mallet, N., Micklem, B. R., Henny, P., Brown, M. T., Williams, C., Bolam, J. P., … , & Magill, P. J. (2012). Dichotomous organization of the external globus pallidus. *Neuron*, *74*(6), 1075–1086.

Mallet, N., Schmidt, R., Leventhal, D., Chen, F., Amer, N., Boraud, T., et al. (2016). Arkypallidal cells send a stop signal to striatum. *Neuron*, *89*(2), 308–316.

Mandali, A., Rengaswamy, M., Chakravarthy, V. S., & Moustafa, A. A. (2015). A spiking basal ganglia model of synchrony, exploration and decision making. *Frontiers in Neuroscience*, *9*, 191. URL https://www.frontiersin.org/article/10.3389/fnins.2015.00191.

Mastro, K. J., Bouchard, R. S., Holt, H. A. K., & Gittis, A. H. (2014). Transgenic mouse lines subdivide external segment of the Globus Pallidus (GPe) neurons and reveal distinct GPe output pathways. *Journal of Neuroscience*, *34*(6), 2087–2099.

Mink, J. W. (1996). The basal ganglia: Focused selection and inhibition of competing motor programs. *Progress in Neurobiology*, *50*(4), 381–425.

Moolchand, P., Jones, S. R., & Frank, M. J. (2017). *Towards a computational account of theta band (4-8 Hz) power modulation in the subthalamic nucleus under response conflict. No. 336.10*. Society for Neuroscience Abstract.

Nevado-Holgado, A. J., Mallet, N., Magill, P. J., & Bogacz, R. (2014). Effective connectivity of the subthalamic nucleus–globus pallidus network during Parkinsonian oscillations. *The Journal of Physiology*, *592*(7), 1429–1455. http://dx.doi.org/10.1113/jphysiol.2013.259721.

Okun, M. S., & Vitek, J. L. (2004). Lesion therapy for Parkinson's disease and other movement disorders: Update and controversies. *Movement Disorders*, *19*(4), 375–389. http://dx.doi.org/10.1002/mds.20037.

Plamen, G., Olivier, D., & Thomas, W. (2006). Oscillations in the basal ganglia under normal conditions and in movement disorders. *Movement Disorders*, *21*(10), 1566–1577. http://dx.doi.org/10.1002/mds.21033.

Planert, H., Berger, T. K., & Silberberg, G. (2013). Membrane properties of striatal direct and indirect pathway neurons in mouse and rat slices and their modulation by dopamine. *PLoS One*, *8*(3), 1–14. https://doi.org/10.1371/journal.pone.0057054.

Prescott, T. J., Gurney, K., & Redgrave, P. (2002). *The basal ganglia: The handbook of brain theory and neural networks* (2nd Ed.). Cambridge: MIT Press.

Prescott, T. J., Montes González, F. M., Gurney, K., Humphries, M. D., & Redgrave, P. (2006). A robot model of the basal ganglia: Behavior and intrinsic processing. *Neural Networks*, *19*(1), 31–61. URL http://www.sciencedirect.com/science/article/pii/S0893608005001589.

Redgrave, P., & Gurney, K. (2006). The short-latency dopamine signal: a role in discovering novel actions? *Nature Reviews Neuroscience*, *7*(12), 967–975.

Redgrave, P., Prescott, T., & Gurney, K. (1999). The basal ganglia: a vertebrate solution to the selection problem? *Neuroscience*, *89*(4), 1009–1023.

Rivlin-Etzion, M., Marmor, O., Heimer, G., Raz, A., Nini, A., & Bergman, H. (2006). Basal ganglia oscillations and pathophysiology of movement disorders. *Current Opinion in Neurobiology*, *16*(6), 629–637. Motor systems/neurobiology of behaviour.

Roessner, V., Plessen, K. J., Rothenberger, A., Ludolph, A. G., Rizzo, R., Skov, L., … , & Hoekstra, P. J. (2011). European clinical guidelines for Tourette syndrome and other tic disorders. Part II: pharmacological treatment. *European Child & Adolescent Psychiatry*, *20*(4), 173–196. https://doi.org/10.1007/s00787-011-0163-7.

Sadek, A. R., Magill, P. J., & Bolam, J. P. (2007). A single-cell analysis of intrinsic connectivity in the rat globus pallidus. *Journal of Neuroscience*, *27*(24), 6352–6362.

Saunders, A., Huang, K. W., & Sabatini, B. L. (2016). Globus pallidus externus neurons expressing parvalbumin interconnect the subthalamic nucleus and striatal interneurons. *PLoS One*, *11*(2), 1–20. https://doi.org/10.1371/journal.pone.0149798.

Schroll, H., & Hamker, F. (2013). Computational models of basal-ganglia pathway functions: focus on functional neuroanatomy. *Frontiers in Systems Neuroscience*, *7*, 122.

Schroll, H., Vitay, J., & Hamker, F. H. (2012). Working memory and response selection: A computational account of interactions among cortico-basalganglio-thalamic loops. *Neural Networks*, *26*(Supplement C), 59–74.

Schultz, W. (1998). Predictive reward signal of dopamine neurons. *Journal of Neurophysiology*, *80*(1), 1–27.

Shine, J. M., Handojoseno, A. M. A., Nguyen, T. N., Tran, Y., Naismith, S. L., Nguyen, H., et al. (2014). Abnormal patterns of theta frequency oscillations during the temporal evolution of freezing of gait in Parkinson's disease. *Clinical Neurophysiology*, *125*(3), 569–576. URL http://www.sciencedirect.com/science/article/pii/S1388245713010420.

Shine, J. M., Matar, E., Ward, P. B., Bolitho, S. J., Gilat, M., Pearson, M., … , & Lewis, S. J. G. (2013). Exploring the cortical and subcortical functional magnetic resonance imaging changes associated with freezing in Parkinson's disease. *Brain*, *136*(4), 1204–1215. http://dx.doi.org/10.1093/brain/awt049.

Stephenson-Jones, M., Samuelsson, E., Ericsson, J., Robertson, B., & Grillner, S. (2011). Evolutionary conservation of the basal ganglia as a common vertebrate mechanism for action selection. *Current Biology*, *21*(13), 1081–1091. URL http://www.sciencedirect.com/science/article/pii/S0960982211005288.

Stewart, T., Bekolay, T., & Eliasmith, C. (2012). Learning to select actions with spiking neurons in the basal ganglia. *Frontiers in Neuroscience*, *6*, 2.

Szydlowski, S. N., Pollak Dorocic, I., Planert, H., Carlén, M., Meletis, K., & Silberberg, G. (2013). Target selectivity of feedforward inhibition by striatal fast-spiking interneurons. *Journal of Neuroscience*, *33*(4), 1678–1683. URL http://www.jneurosci.org/content/33/4/1678.

Tachibana, Y., Iwamuro, H., Kita, H., Takada, M., & Nambu, A. (2011). Subthalamo-pallidal interactions underlying Parkinsonian neuronal oscillations in the primate basal ganglia. *European Journal of Neuroscience*, *34*(9), 1470–1484. https://doi.org/10.1111/j.1460-9568.2011.07865.x.

van Albada, S., & Robinson, P. (2009). Mean-field modeling of the basal ganglia-thalamocortical system. I: Firing rates in healthy and Parkinsonian states. *Journal of Theoretical Biology*, *257*(4), 642–663.

Wahlstrom, D., Collins, P., White, T., & Luciana, M. (2010). Developmental changes in dopamine neurotransmission in adolescence: Behavioral implications and issues in assessment. *Brain and Cognition*, *72*(1), 146–159. URL http://www.sciencedirect.com/science/article/pii/S027826260900205X.

Weinberger, M., & Dostrovsky, J. O. (2011). A basis for the pathological oscillations in basal ganglia: the crucial role of dopamine. *Neuroreport*, *22*(4), 151–156. URL http://www.ncbi.nlm.nih.gov/pmc/articles/PMC3076312/.

Wilson, C. J., & Groves, P. M. (1981). Spontaneous firing patterns of identified spiny neurons in the rat neostriatum. *Brain Research*, *220*(1), 67–80. URL http://www.sciencedirect.com/science/article/pii/0006899381902110.

Wylie, S., van den Wildenberg, W., Ridderinkhof, K., Bashore, T., Powell, V., Manning, C., et al. (2009). The effect of Parkinson's disease on interference control during action selection. *Neuropsychologia*, *47*(1), 145–157.

Yoon, D. Y., Gause, C. D., Leckman, J. F., & Singer, H. S. (2007). Frontal dopaminergic abnormality in Tourette syndrome: A postmortem analysis. *Journal of the Neurological Sciences*, *255*(1), 50–56. URL http://www.sciencedirect.com/science/article/pii/S0022510X07000949.

Zhang, J., Russo, G. S., Mewes, K., Rye, D. B., & Vitek, J. L. (2006). Lesions in monkey globus pallidus externus exacerbate Parkinsonian symptoms. *Experimental Neurology*, *199*(2), 446–453. URL http://www.sciencedirect.com/science/article/pii/S0014488606000136.